



## Stability study of aqueous foams under high-temperature and high-pressure conditions relevant to Enhanced Geothermal Systems (EGS)<sup>☆</sup>

Viren Thakore <sup>a,b,\*</sup>, Hong Wang <sup>b</sup>, Jy-An Wang <sup>b</sup>, Yarom Polsky <sup>c</sup>, Fei Ren <sup>a</sup>

<sup>a</sup> Department of Mechanical Engineering, Temple University, Philadelphia, PA, 19122, USA

<sup>b</sup> Materials Science & Technology Division, Oak Ridge National Laboratory, Oak Ridge, TN, 37831, USA

<sup>c</sup> Manufacturing Science Division, Oak Ridge National Laboratory, Oak Ridge, TN, 37831, USA



### ARTICLE INFO

**Keywords:**

Enhanced Geothermal System (EGS)

Foam fracturing fluid

Stabilizing agent

High-temperature

High-pressure

Activation energy

Drainage rate

Molar volume

### ABSTRACT

In Enhanced Geothermal System (EGS) hydraulic fracturing is carried out by injecting cold water into deep Hot Dry Rocks (HDR) under carefully controlled conditions to create new or reopen existing fractures. Water-based fracturing fluids demonstrate some challenges including immense quantity of water usage, water sensitivity of the formations, water blocking, and lack of proppant carrying capacity and transportation. Thus, an alternative is to use foam-based fracturing fluid which offers potential advantage over conventional water-based fracturing fluid such as minimum water usage, reduced wellbore damage, high proppant carrying capacity, and less environmental damage. However, foams are complex mixture of gaseous phase and liquid phase which are thermodynamically unstable at downhole conditions, and their stability can decrease over time due to liquid drainage, bubble coarsening, and coalescence. This paper shows laboratory experiments executed to study foam stability at high temperature (200 °C) and high pressure (6.9 MPa) conditions which simulates the geothermal environment. Foam stability was characterized by half-life of foam, which is defined as the time taken by the foam to decreases by 50% of its original height due to drainage. In this paper, two types of gaseous phases, nitrogen (N<sub>2</sub>) and carbon dioxide (CO<sub>2</sub>) were investigated. Also, based on successful practice of foam-based fracturing fluid in oil and gas industries, four surfactants, including Alpha olefin sulfonate (AOS), Sodium dodecyl sulfonate (SDS), Tergitol™ (NP – 40), and Cetyltrimethylammonium chloride (CTAC) at optimum concentration of 1 wt.% were tested for best stability performance. In addition, different stabilizing agents including guar gum, bentonite clay, crosslinker, silicon dioxide nanoparticles (SiO<sub>2</sub>), graphene oxide (GO) were also studied. Experimental results showed that N<sub>2</sub> foams were more stable than CO<sub>2</sub> foams. It was observed that foam half-life decreased with the increase in temperature. Among all the surfactants, AOS foams showed the most promising thermal stability at high temperatures. Moreover, with the addition of stabilizing agents, foam's half-life was enhanced. Stabilizing agents such as crosslinker and GO dispersion showed the most stable foams with half-life recorded at 20 min and 17 min, respectively, at 200 °C and 6.9 MPa. Finally, pressure also showed a positive effect on foam stability; with increased pressure, foam half-life was increased. Based on the experimental data, analytical models for the effect of temperature and pressure were developed, considering foam degradation is a first-order kinetic reaction that linearly depends on the foam drainage mechanism. The effect of temperature on foam half-life was studied as an exponential decay model. In this model, foam half-life is a function of drainage rate constant ( $D_A$ ) and activation energy ( $E_a$ ) of the foam system. The effect of pressure on foam half-life was found to obey a power-law model where an increase in pressure showed an increase in foam half-life. Furthermore, a linear relation was studied for the effect of pressure on foam activation energy and drainage rate. Then the combined effects of temperature and pressure were studied, which yielded an analytical model to predict the foam stabilities in terms of half-life for different foam compositions. This research indicates that with an appropriate selection of surfactants and stabilizing agents, it is possible to obtain stable foams, which could replace conventional water fracturing fluid under EGS conditions.

<sup>☆</sup> This manuscript has been co-authored by UT-Battelle, LLC, under contract DE-AC05-00OR22725 with the US Department of Energy (DOE). The publisher acknowledges the US government license to provide public access under the DOE Public Access Plan (<http://energy.gov/downloads/doe-public-access-plan>).

\* Corresponding author.

E-mail address: [thakorev@temple.edu](mailto:thakorev@temple.edu) (V. Thakore).

## 1. Introduction

Geothermal energy is clean, sustainable, and renewable energy that can be found abundance on our planet, which is widely considered to be a practical alternative energy source. This vast thermal energy is stored in Hot Dry Rocks (HDR) that are present 2–3 miles (10,560 ft – 15,840) underneath the earth surface. In recent years hydrofracking of HDR have become growing interest in Enhanced Geothermal System (EGS). EGS is defined as extracting heat form HDR by injection of high-pressure fracturing fluid under carefully controlled condition and creating effective fracture networks that can be circulated and heated (Lu, 2018).

In development of EGS, fracturing fluid is an important component that not only concerns the technical approach but also environmental impact. Fracturing fluids are typically water-based fluids, which can cause formation damage, harm the environment due to high volume of water usage, and contaminates surface water resources by usage of additives (Gaurina-Medimurec et al., 2021; Barati and Liang, 2014; Huang, 2018). Also, It is anticipated that the regulations have significantly increased with use of water-based fracturing fluid (Olasolo et al., 2016; Reber et al., 2014; Clark et al., 2010). All these factors leads to development of waterless fracturing technologies that could help in addressing these concerns especially in regions where water resource is a challenge (Kohshou et al., 2017; Mordis and George 2017; Gandossi, 2016). Waterless fracturing has been already explored for more than 40 years in oil and gas industries which covers a wide range of mechanical, electrical, and chemical fracturing methods. Among all waterless fracturing techniques, foam-based fracturing has gained great interest in EGS application (Gandossi, 2016; Wang et al., 2019; Wanniarachchi et al., 2017).

Foam fracturing has already been practiced by oil and gas industries to fracture low permeability reservoirs like shale. Study showed that foam-based fracturing fluid were less expensive, more effective with ultra-high quality foams, has high proppant carrying capacity, showed reduced formation damage with effective fracture growth, improved well performance, and enhanced productivity of fractured wells when compared to conventional water-based fracturing fluid (Frohne, 1976; Riedel, 1981; Wanniarachchi et al., 2015; Oussoltsev et al., 2008; Yekeen et al., 2018). Although foam fracturing has been carried out in the oil and gas industries for many years, relatively less advancement is achieved in EGS applications. So far, foam fracturing have only been investigated in laboratory experiments with combination of finite element analysis for understanding foam fluid rheological properties at reservoir conditions (Wang et al., 2021; Wilk, 2019; Lai et al., 2018). However, there are no EGS sites with foam fracturing yet as foams are confronted by foam instability due to earth stresses and temperature what are generally higher than those seen in oil and gas.

Foams are complex mixtures of liquids with a gaseous phase, where the liquid phase act as an ambient phase and gas as the dispersed phase. Foam rheological properties are critical for EGS hydrofracking including viscosity, density, and stability (Faroughi et al., 2018). For EGS application performance of foam is extremely influenced by the downhole condition that involves high temperatures and high pressures. One of the important rheological properties for making foam-based fracturing fluid a viable alternative is foam stability. The stability of foams at high temperatures ( $> 150^{\circ}\text{C}$ ) is not well understood partly because most existing applications, such as those used in the oil and gas industries, only involve services at relatively low temperatures (below  $150^{\circ}\text{C}$ ). Stability of foam depends on slowing down three major phenomenon taking part in foam bubbles these are described as: coarsening, coalescence, and drainage (Thomas, 2015; Georgieva et al., 2009; Saint-Jalmes, 2006). All the three phenomena are inter-related, where controlling drainage can influence both coarsening and coalescence.

Stable foams require surfactants (foaming agents) and stabilizing agents (additives) that can survive at geothermal environment. Researchers have developed laboratory-scale experimental setups that resembles geothermal environment to study foam rheological properties

involving different gaseous phase, surfactants, stabilizing agents at downhole conditions. One of the studies evaluated different classes of surfactants to measure the foam half-life at a temperature of  $65^{\circ}\text{C}$  (H. Wang et al., 2017), they showed that the half-life of all the foams decreased with an increase in temperature, also anionic surfactants were found to be the best foaming agent in terms of foam stability compared to cationic and non-ionic surfactants (Y. Wang et al., 2017). One of the early research tested 50 different surfactants exposed to  $260^{\circ}\text{C}$  down-hole condition to determine if foam can survive, among those surfactants alpha olefin sulfonates as a class appears to be best performing surfactant available for geothermal application (Rand and Montoya, 1983). Surfactant selection for a given application will depend on cost, anticipated chemical environment, compatibility with corrosion inhibitors, and stability of aqueous foams. Several laboratories scaled experiments have studied foam stability with only surfactants for EGS applications which showed that, the apparent viscosity of foam decreased as the temperature increased and at high temperature low viscosity is believed to be the main influence causing rapid liquid drainage for unstable foams (Thakore et al., 2020; Ahmed et al., 2018; Chen et al., 2014; Chen et al., 2016). The viscosity of the liquid phase directly affects the foam stability, the higher the viscosity, the longer lasting, and more stable foams are. Therefore, one way to enhance the stability of liquid foams is by the addition of stabilizing agents. A substantial amount of laboratory scale experiments have been conducted to test stabilizing agents such as guar gum and crosslinker agents (guar gum with addition of borate salts) to test enhanced foam stability at geothermal conditions (Harris and Reidenbach, 1987; Harris, 1993). Addition of these stabilizing agents increase the viscosity of the foam base fluid and with increase in concentration of stabilizing agents foam stability was increased at a given temperature (Miller, 2005). Several other literatures showed positive effect of different types of stabilizing agents on foam stability at high temperature due to the adsorption of a polymer layer of surfactant onto the gelling agent (guar/bentonite clay) particle surface which results in better stabilization of bubbles (Verma et al., 2017; Zhang et al., 2019; Thakore et al., 2021).

Thermal stability of foam with addition of nanoparticles have also been investigated at downhole conditions. The presence of nanoparticle aggregates at plateau border of foam bubbles to stop free drainage of foam by trafficking. The concentration of nanoparticles, salinity of solution, and their charges are all important parameters that affect the rheological behavior of these foam fracturing fluids. Several literature experiments on Silicon dioxide ( $\text{SiO}_2$ ) nanoparticles have already proved the worth of understanding the nanoparticle stability and its proppant carrying capacity to keep fracture open and enhance well productivity which is important for EGS application (Emrani and Nasr-El-Din, 2017; Lv et al., 2015; Al-muntasher et al., 2017). In addition to  $\text{SiO}_2$  nanoparticles, graphene oxide dispersion (GO) was also considered to be a foam additive for enhanced oil recovery. GO is considered to adhere by a lower interfacial energy which acts like a surfactant and capable of stabilizing oil-water interface to form the particles-stabilized emulsions (Cote et al., 2011; Kim et al., 2010), moreover GO as stabilizing agent has good hydrophilicity and the highest interfacial activity that enabled stabilizing foams (Barrabino et al., 2018). Few literatures have experimentally investigated the combined effect of temperature and pressure on foam stability by recoding its life-time. Studies have shown that temperature will destroy foam stability, while pressure effect enhanced foam stability, which can be explained by an increase in the Marangoni effect that allows liquid to flow from areas with lower surface tension to areas with higher surface tension (Szabries et al., 2019; Maini and Ma, 1986).

To date, there is very limited information on the thermal stability of liquid foams at elevated temperatures (e.g.,  $150^{\circ}\text{C}$  and above), which are typical in EGS environments. In this research experiments were conducted using laboratory equipment that demonstrates downhole condition to measure foam life span with different surfactants and stabilizing agents. Results indicate that, foam stability is known to decrease

with increase in temperature, however foams are highly stable with addition of stabilizing agents and high injection pressure. This paper also manifests first layout for analytical model for effect of temperature and pressure on foam half-life as exponential decay and power models respectively. This model will provide guidelines for design of stable foams and predict its rheological behavior for EGS foam fracturing application.

## 2. Experimental method

### 2.1. Foam generator equipment

A laboratory-based foam generator was designed and constructed to study foam stability under controlled conditions. A schematic of foam stability setup is illustrated in Fig. 1.

### 2.2. Foam base solutions

Foam base solution is the liquid phase of the generated foam which is typically mixture of water and surfactant/stabilizing agent stored in the stainless-steel tank. In this study foam-based solution is a mixture of Deionized water (DI) with an optimum concentration of surfactant/stabilizing agent. Four different surfactants and five types of additives were investigated in this study. The surfactants studied for foam stability were Alpha Olefin Sulfonate (AOS), Sodium Dodecyl Sulfate (SDS), Tergitol™ (NP-40), and Cetyltrimethylammonium Chloride (CTAC), respectively which are well known in shale foam fracturing for oil and gas industries (Ahmed et al., 2018; Ahmed et al., 2017; Gu and Mohanty, 2015; Ranjani and Ramamurthy, 2010; Bera et al., 2017). All the surfactants are differentiated based on their ionic groups, AOS and SDS are commonly used anionic surfactants with negative hydrophilic end, NP-40 is a non-ionic polyoxymethylene surfactant (long chain of alcohol), and CTAC is a cationic surfactant which comprises of positively charged hydrophilic head. Various stabilizing agents studied based on literature were guar gum, bentonite clay, crosslinking agent (guar + borate salt), silicon dioxide nanoparticles (60–70 nm size), and graphene oxide dispersion (Verma et al., 2017; Li et al., 2016; Ranka et al., 2015) All these chemicals were purchased from commercial sources and

diluted to the specific concentration to make the base solutions (Table 2.1). In the current study, all surfactants were tested at 1 wt.% concentration, which was a common value used in many literatures work, it has been shown when the concentration of the surfactant was above an optimal value, no significant increase in stability could be observed (Simjoo et al., 2013; Azdarpour et al., 2013). Fig. 2 represents samples of the foam base solutions prepared in this study.

### 2.3. Operating the high-pressure and high-temperature foam generator

In a typical experiment, foam generation is initiated from a base solution. The foam base solution is stored in a 6-liter stainless steel tank; from there it is pumped to the liquid line through an air-driven pump. The pressurized base solution is controlled through the pressure regulator before passing the accumulator, which stabilizes the fluctuating pressure from the air-driven pump. Simultaneously, the gas tank is kept open, and gas pressure is controlled with a two-stage pressure regulator. The liquid flow and gas flow are controlled by a high-pressure rated liquid flow meter and gas flow meter, respectively. The flow meter helps control the foam quality, which is the ratio of gas volume to foam volume; in this research, foam stability is studied at ~90% quality (10 vol%

**Table 2.1**  
Surfactants and stabilizing agents tested in this study.

Chemical name	Type	Vender	Concentration (wt.%)
AOS	Surfactant (anionic)	Sigma-Aldrich	1
SDS	Surfactant (anionic)	Sigma-Aldrich	1
NP-40	Surfactant (non-ionic)	Sigma-Aldrich	1
CTAC	Surfactant (cationic)	Sigma-Aldrich	1
Guar gum	Gelling agent	Sigma-Aldrich	0.36
Bentonite clay	Gelling agent	Sigma-Aldrich	0.36
Borate salt	Cross-linker	Sigma-Aldrich	0.1
SiO <sub>2</sub>	Nanoparticle, 50–70 nm	US research Nanomaterials	0.1
Graphene oxide	Nanoparticle, 4–30 μm (lateral size)	Graphenea	0.05

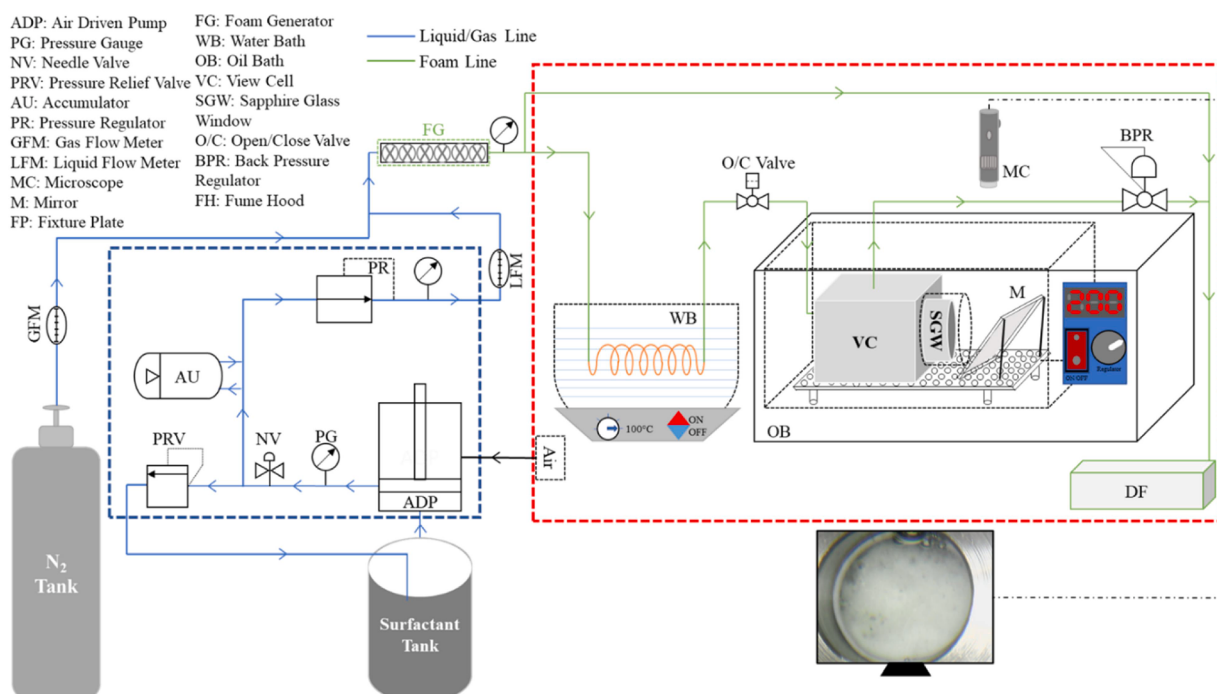


**Fig. 1.** Schematic of High-Pressure and High-Temperature foam stability study.

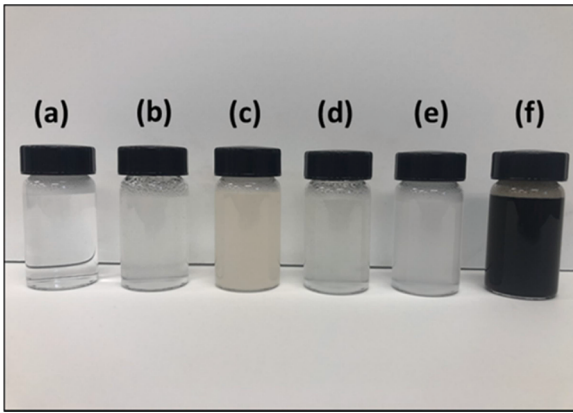


**Fig. 2.** Picture showing samples of foam base solutions containing a) AOS, b) AOS + guar gum, c) AOS + clay, d) AOS + crosslinker, e) AOS + SiO<sub>2</sub>, and f) AOS + GO.

of water in foams), which is also termed as high-quality foams. After passing through their respective pressure regulators and flow meters, the high-pressure liquid line and gas line meet up at a TEE junction to generate foam in the foam generator tube, as shown in the schematic Fig. 1. After, the foam is generated is passed towards the high-temperature system for foam stability measurements.

#### 2.4. Foam half-life measurement

The foam life is measured inside the view cell at a given temperature and pressure condition to study the foam stability. Before the foam is injected, the view cell is first heated to reach the oil bath temperature, which is checked with an IR camera. The foam quality is controlled by adjusting the flow rates of gaseous and liquid phases, and pressure regulators control foam injected pressure. It is important to note that the injection of foams into the view cell would slightly reduce the temperature due to the lower temperature of the foams. This phenomenon may represent a potential temperature drop in the HDR because of the injection of ambient-temperature fluid. This “quenching” effect in the view cell was partially mitigated by preheating the foam using the water bath.

The foam is injected into the view cell and then monitored by a digital camera as shown in Fig. 3(a). By measuring the foam height as a function of time, the half-life of the foam, i.e., the time needed to reduce to 50% of the original foam height, can be determined (Fig. 3(b)). For each testing condition, three experiments were conducted, and the average values were reported. Fig. 4 shows some example data for N<sub>2</sub> foams, where the normalized foam height as a function of time was plotted at various temperatures. The half-life of the foam was determined by finding the time corresponding to 50% of the initial foam height (see the red dotted line as an example).

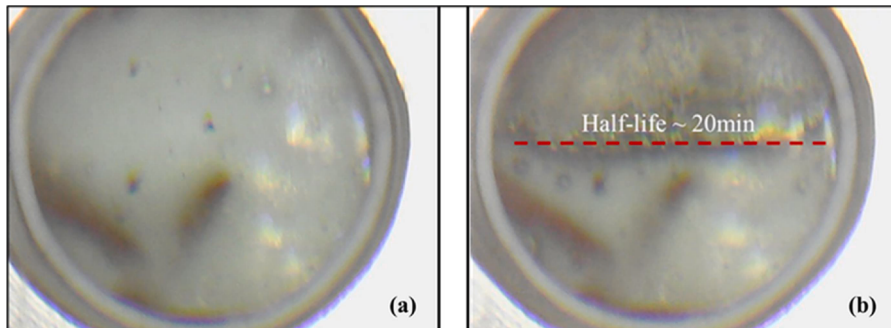


**Fig. 3.** AOS + Crosslinker foam at 200 °C and 6.9 MPa. The two images represent foam (a) after injection and (b) at 50% height.

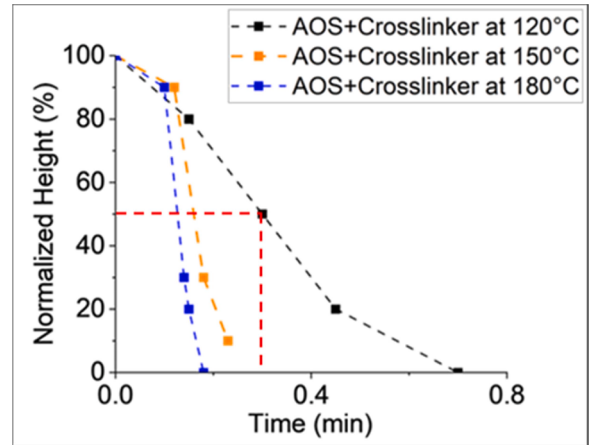


**Fig. 4.** Foam Height measurement to time for AOS + Crosslinker foams at various temperatures.

### 3. Results & discussion

In this section, experimental results and data for foam half-life are reported. Focus on the gaseous phase, surfactants, and stabilizing agents will be elaborated. The effect of temperature and pressure on foam stability will be investigated based on experimental data.

#### 3.1. N<sub>2</sub> versus CO<sub>2</sub> foams

Foam stability for N<sub>2</sub> and CO<sub>2</sub> gaseous phase were tested with surfactant only at room temperature and 100 °C with foam generation pressure of 30 psi. These test results were significant for the future experiment considering the type of gaseous phase. Fig. 5 illustrates foam stability performance by comparing the half-life of different surfactants with N<sub>2</sub> and CO<sub>2</sub> as dispersed/gaseous phases at room temperature and 100 °C.

The results show that the half-life variations of N<sub>2</sub> foams and CO<sub>2</sub> foams as a function of surfactant types are similar when compared between at room temperature. In both phases, AOS foams are the least stable, and NP-40 foams are the most stable. Interestingly, increased temperature resulted in a changed variation pattern; it was observed that AOS foams were more stable with N<sub>2</sub> foams, while with the CO<sub>2</sub> gas gaseous phase, all the surfactant-based foams showed a similar half-life.

Foams with N<sub>2</sub> as the gaseous phase were much more stable with than CO<sub>2</sub> at room temperature. Foams made with N<sub>2</sub> had half-lives higher than 50 min, while CO<sub>2</sub> foams had half-lives between 6 and 10 min. As expected, with increased temperature, thermal stability drastically decreased for both the gaseous phases. But the half-lives of N<sub>2</sub> foams were still recorded a little higher than that of CO<sub>2</sub>. Overall, the foam of N<sub>2</sub> and AOS displayed the longest half-life of around 0.45 min.

Thus, the nature of the gaseous phase used for foam generation plays

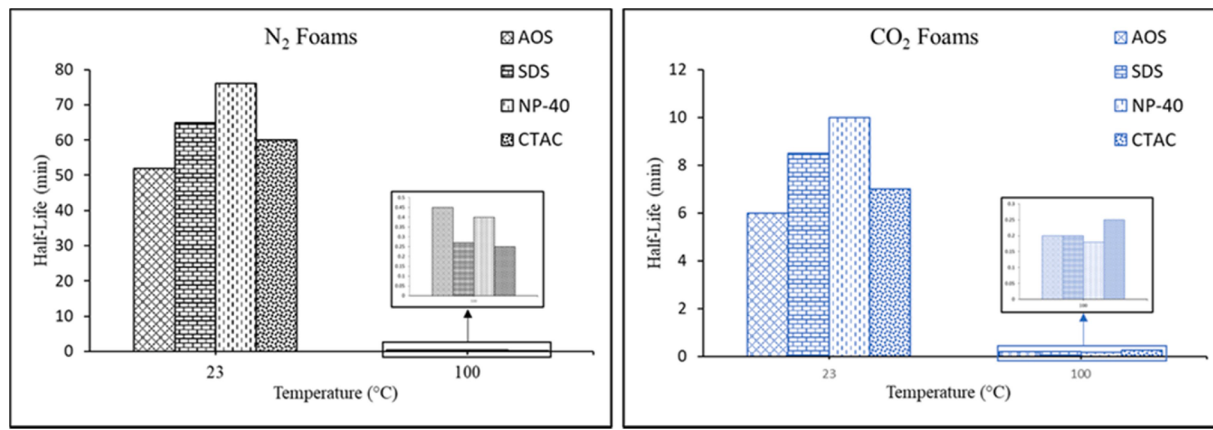


Fig. 5. Thermal stability of foams with Nitrogen (N<sub>2</sub>) and Carbon dioxide (CO<sub>2</sub>) for different surfactants.

a vital role in determining its stability. A recent study on the effect of the gaseous phase on foam stability also investigated foam stability with CO<sub>2</sub> and N<sub>2</sub> gaseous phases. Their results confirmed that foam generated with N<sub>2</sub> gas has the maximum stability compared to CO<sub>2</sub> foams (Alooghereh et al., 2021). CO<sub>2</sub> foams were less stable than N<sub>2</sub> foam, which may be explained by the higher solubility of CO<sub>2</sub> that can lead to faster transport across the bubble films resulting in faster drainage and thus shorter half-life (Rio et al., 2014). These results were significant for gaseous phase selection in the future analysis of foam stability at high pressure and temperature, considering the geothermal environment. Thus, further investigation on foam stability was recorded using N<sub>2</sub> as a gaseous phase for different surfactants and stabilizing agents.

### 3.2. Stability of N<sub>2</sub> foams containing AOS and stabilizing agents

AOS is an anionic surfactant commonly included in the base fluids as fracturing fluid used by oil and gas industries. Fig. 6 shows the half-life of various AOS foams with and without gelling/ stabilizing agent at different temperatures and pressures. For all compositions, it is observed that foam half-life decreases with an increase in temperature. On the other hand, the half-life is increased with an increase in pressure. The half-life of AOS+Crosslinker foam decreased from 60 min to 0.8 min when the temperature increased from 100 °C to 200 °C. Whereas at 200 °C, with the increase in pressure from 0.69 MPa to 1.38 MPa, the half-life of AOS foam is observed to increase from 0.45 min to 1 min. Adding other stabilizing agents further enhanced the thermal stability of AOS foams, which is more prominent at pressures above 1.38 MPa. Crosslinking agents (borate salts) and graphene oxide nanoparticles

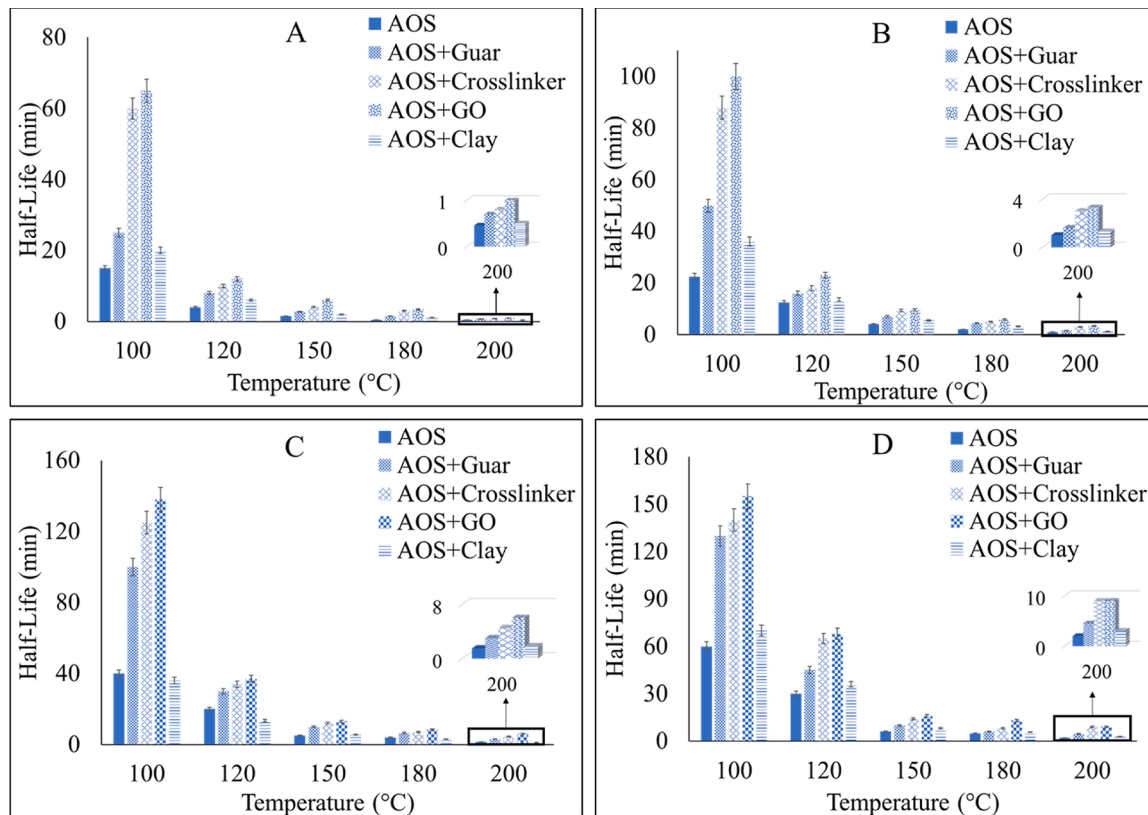


Fig. 6. Half-life of AOS foams with different stabilizing agents at (A) 0.69 MPa, (B) 1.38 MPa, (C) 2.07 MPa, and (D) 2.76 MPa.

generated the most stable AOS foams, which showed similar thermal stability at high temperature and pressure; their half-life was found to be around 9 min at 200 °C and 2.76 MPa. Gelling agent guar gum also enhanced thermal stability for AOS foams, recording stable foams for approximately 4.5 min at 200 °C and 2.76 MPa. At 2.76 MPa and 200 °C, the foam half-life was measured to be about 3 min with the addition of bentonite clay, which among all the stabilizing agents was the least effective and showed similar thermal stability behavior to that of only AOS foams.

### 3.3. Stability of N<sub>2</sub> foams containing SDS and stabilizing agents

SDS is another anionic surfactant capable of generating long-lasting room temperature foams. As shown in Fig. 7, the thermal stability of SDS foam decreased with an increase in temperature, and a drastic reduction in half-life is observed for temperatures above 120 °C. At 200 °C, the half-life of SDS foam increased from around 0.13 min at 0.69 MPa to about 0.41 min at 2.76 MPa. On the other hand, at 2.76 MPa, SDS foam's half-life plunged by 33% with an increase in temperature from 100 °C to 200 °C. The addition of gelling agent guar gum showed enhanced thermal stability compared to only SDS foams at 100 °C, which recorded a 23% increase at 0.69 MPa compared to a 16% increase at 2.76 MPa. SDS with the addition of guar gum foams were observed to have a half-life of only 0.5 min at 200 °C and 2.76 MPa. SDS foam with the addition of graphene oxide showed the best stability at the temperature of 100 °C under all pressure ranges. SDS+GO foam's half-life at 100 °C was recorded at 10 min and increased to 23 min with an increase in pressure from 0.69 MPa to 2.76 MPa. GO foams recorded a half-life of 0.9 min at 200 °C and 2.76 MPa. SDS foams with the addition of bentonite clay half-life were recorded at 0.75 min for 2.76 MPa and 200 °C. Cross-linking agent borate salt showed the least stable foams at 200 °C for pressure up to 2.07 MPa. However, with an increase in pressure to 2.76

MPa, this foam showed a similar half-life as GO and clay foams.

### 3.4. Stability of N<sub>2</sub> foams containing NP-40 and stabilizing agents

Foams containing only NP-40 showed a radical decrease in thermal stability with an increase in temperature above 120 °C. From Fig. 8, NP-40 foam showed an 83% increase in half-life with an increase in pressure at 100°, while at 200 °C, NP-40 foams recorded an 85% increase with an increase in pressure from 0.69 MPa to 2.76 MPa. NP-40 foams were observed to have a half-life of roughly 0.5 min at 0.69 MPa. However, when the temperature was increased from 100 °C to 200 °C, the half-life decreased by 57% but only slightly at 2.76 MPa. All stabilizing agents showed a similar half-life at the pressure range of 0.69 MPa and 1.38 MPa. With the increase in pressure, NP-40 + GO generated the most stable foams. At 200°C, NP-40 + GO foam's half-life was recorded at 0.5 min, 0.6 min, 1.8 min, and 2.8 min under 0.69 MPa, 1.38 MPa, 2.07 MPa, and 2.76 MPa, respectively. On the other hand, bentonite clay was the least effective stabilizing agent with an increase in pressure with a half-life of 0.7 min and 1.5 min at 200 °C at 0.69 MPa and 2.76 MPa, respectively. The half-life of foams with guar and crosslinker stabilizing agent was recorded at 1.7 min, and 2 min at 200 °C and 2.76 MPa, respectively.

### 3.5. Stability of N<sub>2</sub> foams containing CTAC and stabilizing agents

CTAC is a cationic surfactant widely used in many fields, such as cosmetics, textile, and petrochemical industries. Fig. 9 shows the effect of the half-life of CTAC foam with different stabilizing agents with increasing in temperature at different injection pressure. A drastic decrease in half-life is observed with an increase in temperature above 120 °C for all CTAC foams. Contrastingly, the half-life increased with an increase in pressure from 0.69 MPa to 2.76 MPa. Stabilizing agent guar

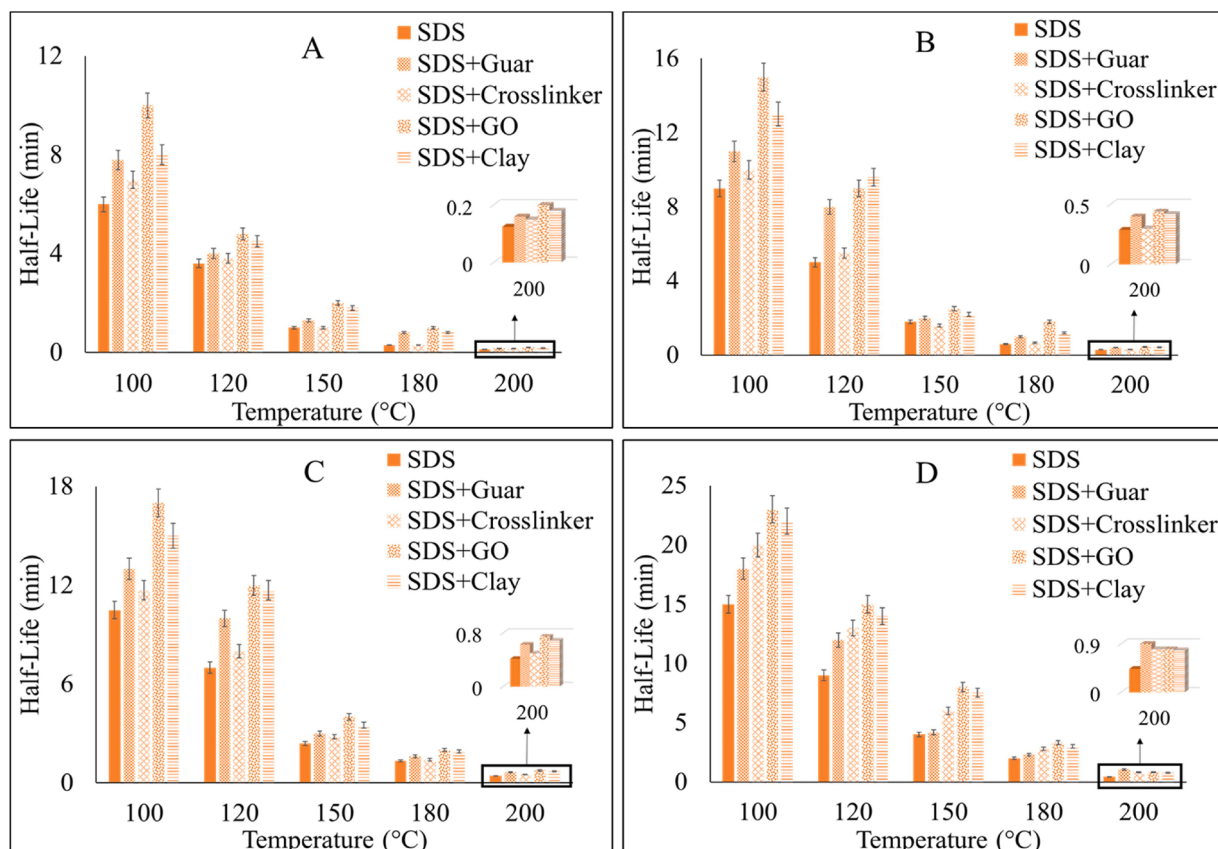


**Fig. 7.** Half-life of SDS foams with different stabilizing agents at (A) 0.69 MPa, (B) 1.38 MPa, (C) 2.07 MPa, and (D) 2.76 MPa.

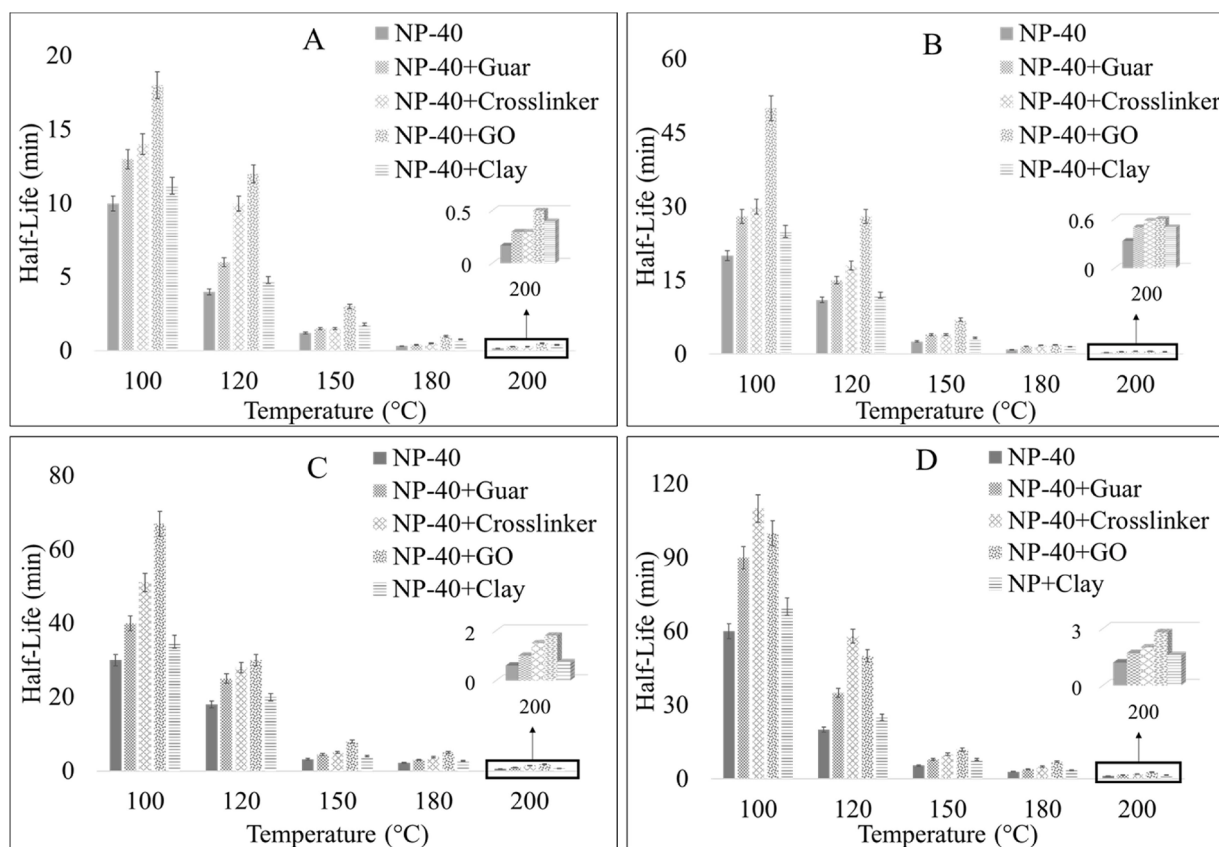


**Fig. 8.** Half-life of NP-40 foams with different stabilizing agents at (A) 0.69 MPa, (B) 1.38 MPa, (C) 2.07 MPa, and (D) 2.76 MPa.

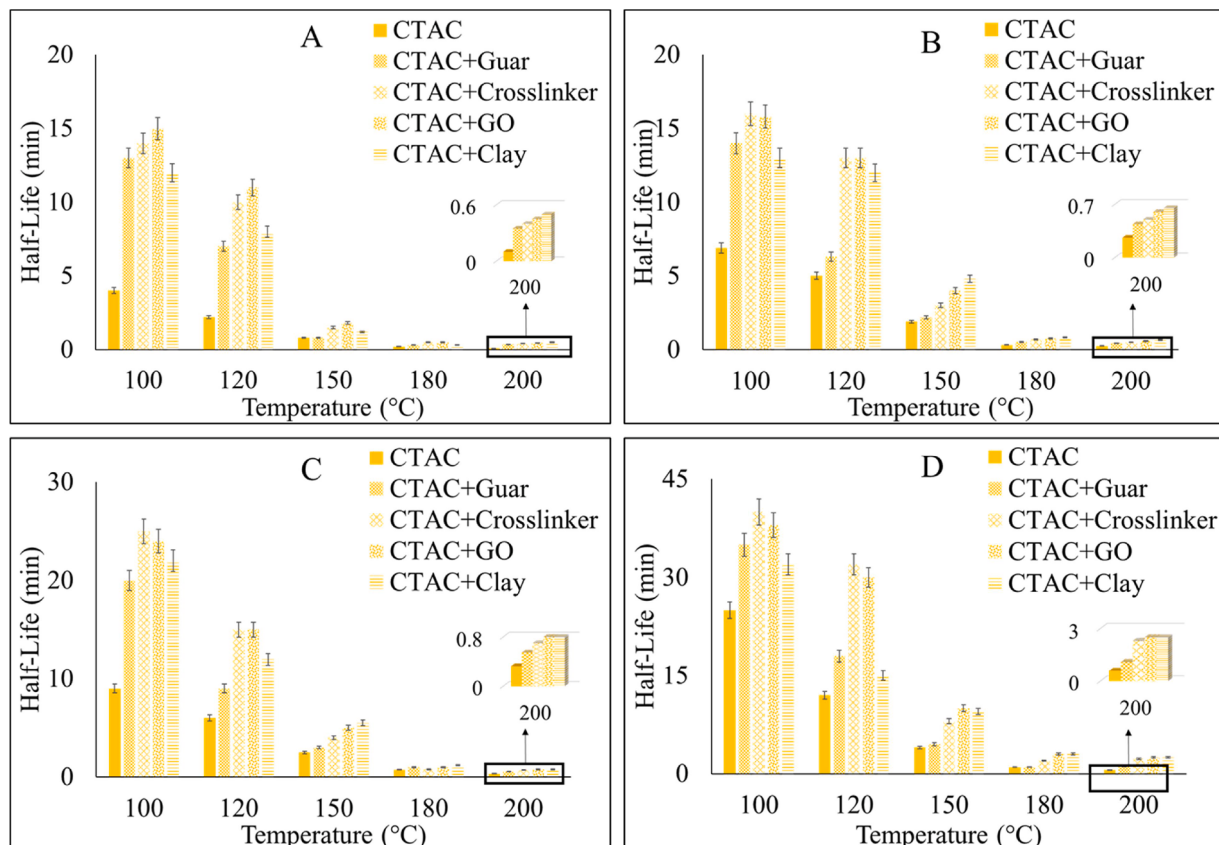


**Fig. 9.** Half-life of CTAC foams with different stabilizing agents at (A) 0.69 MPa, (B) 1.38 MPa, (C) 2.07 MPa, and (D) 2.76 MPa.

gum can significantly stabilize CTAC foams at a temperature of 100 °C and 120 °C but is observed to be the least stable at a higher temperature above 150 °C. The crosslinker agent was the most effective stabilizing agent for all the pressure ranges. However, thermal stability rapidly decreased with an increase in temperature with a half-life of 40 min at 100 °C, which was then reduced to 2 min at 200 °C at 2.76 MPa. Graphene oxide enhanced thermal stability for CTAC foam at 200 °C, with a half-life of 0.45 min, 0.6 min, 0.8 min, and 2.5 for 0.69 MPa, 1.38 MPa, 2.07 MPa, and 2.76 MPa, respectively. Also, stabilizing agent bentonite clay showed a drastic increase in stability at high temperatures and pressure. It was observed that the thermal stability of CTAC foam was significantly enhanced with the addition of clay and GO stabilizing agents showing an 80% increase in half-life at 200 °C compared to CTAC-only foams.

Thermal stability of aqueous nitrogen foams in the temperature range between 100 °C and 200 °C with injection pressure varied between 0.69 MPa and 2.76 MPa was initially examined. Foams stabilized with four surfactants and other stabilizing agents, including guar gum, bentonite clay, crosslinker, and GO, were examined. Results indicated that foam half-life decreased sharply with an increase in temperature. On the other hand, foams became relatively more stable as pressure increased. Half-life data recorded so far were at 200 °C; however, the injection pressure is not close to what is needed during the foam fracturing process. So far, the above half-life results helped distinguish potential surfactant and stabilize agents for further analysis, closely related to downhole geothermal environment conditions. At this range of pressure and temperature, among all the surfactants, AOS foam showed the best overall stabilizing effect.

Thus, further experiments on AOS foam stability at high pressure up to 6.9 MPa and high temperature of 200 °C, which closely resemble the geothermal environment, were conducted on AOS foams with different stabilizing agents. Later analytical model was developed based on high temperature and high pressure AOS foams half-life.

### 3.6. AOS foams stability at high temperature and high pressure

AOS foam stability was tested with different stabilizing agents for a temperature of 100 °C and 200 °C and pressure range of 0.69 MPa to 6.9 MPa. Fig. 10 shows the half-life of all AOS foams at increasing pressure range for 100 °C and 200 °C.

A general increasing trend was observed as the pressure increased from 0.69 MPa to 6.9 MPa for both the temperature ranges. For only AOS foams at 100 °C, the half-life at 6.9 MPa reached 78 min, more than four times the increase over the value measured at 0.69 MPa. A monotonic increase in half-life as a function of pressure was also observed at 200 °C,

and the half-life of AOS foams increased from 0.5 min at 0.69 MPa to 10 min at 6.9 MPa. When comparing the data points taken at the same pressure, half-lives recorded at 200 °C were shorter than those taken at 100 °C, as expected.

The half-life of guar foams at 100 °C and 0.69 MPa was recorded at 30 min, and with the increase in pressure to 6.9 MPa, the half-life increased to 170 min, which are 66% and 120% higher than the AOS-only foams at 0.69 MPa and 6.9 MPa, respectively. At 200 °C, guar foams lasted only a few minutes under 0.69 MPa. However, with the increase in pressure to 6.9 MPa, its half-life was increased by 20 times to 15 min. When temperature increases from 100 °C to 200 °C, the half-life decreases by 90% at both pressure ranges of 100 and 6.9 MPa, respectively.

The half-life of clay foams at 100 °C increased by 450% from 20 min at 0.69 MPa to 110 min at 6.9 MPa. At 100 °C and 6.9 MPa, the half-life of clay foam was 40% longer than that of AOS-only foam. At 200 °C, the half-life was also observed to increase from ~ 1 min at 0.69 MPa to nearly 15 min at 6.9 MPa. Compared to AOS-only foams, the half-life increased by 50% at 6.9 MPa. Foam stability also decreased for clay foams with an increase in temperature from 100 °C to 200 °C; at 0.69 MPa and 6.9 MPa, the half-life of foams decreased drastically by 90% and 80%, respectively.

The half-life of crosslinker foams at 100 °C and 0.69 MPa were recorded at 60 min and increased to 190 min at 6.9 MPa, representing a 200% increase. At 200 °C and an increase in pressure from 0.69 MPa to 6.9 MPa, crosslinker foam's half-life was recorded to increase from 0.8 min to 20 min, which is a 2000% increase in half-life. Crosslinker foams showed enhanced foam stability performance compared to guar gum and bentonite clay at a temperature of 200 °C. At 200 °C and 6.9 MPa, crosslinker foam half-life increased by 150% compared to only AOS foams. However, crosslinker foams also showed decreasing foam stability with increasing temperature from 100 °C to 200 °C. Crosslinker foam half-life is observed to decrease by 98% and 90% at injection pressures of 100 psi and 6.9 MPa, respectively, with an increase in temperature to 200 °C.

At 100 °C, the half-life of SiO<sub>2</sub> foams was recorded at 6.9 MPa was at 150 min, which showed an increase of 150% when the pressure was 0.69 MPa. At a high temperature of 200 °C, SiO<sub>2</sub> also showed promising performance where foam half-life reached 17 min at 6.9 MPa, which was a 145% increase compared to 0.69 MPa. Compared to AOS-only foams at 200 °C and 6.9 MPa, the half-life was increased by 75% with the addition of SiO<sub>2</sub> nanoparticles. However, half-life decreased with an increase in temperature. It is observed that the half-life decreases with increasing temperature and pressure. As temperature increases from 100 °C to 200 °C and 0.69 MPa to 6.9 MPa, the half-life decreases by 90% and

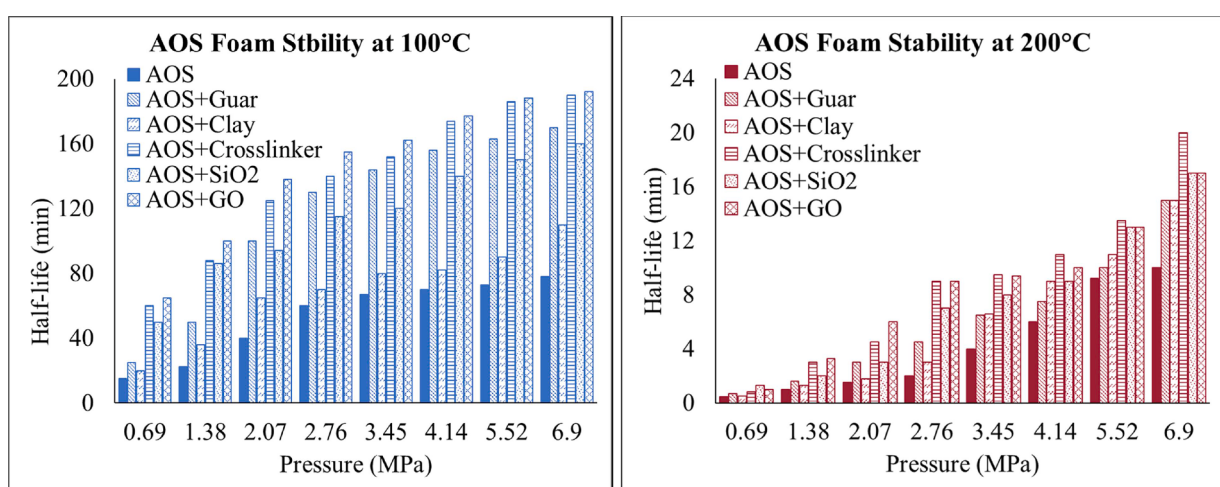


**Fig. 10.** Comparing half-life of AOS foams with different stabilizing agents for 100 °C and 200 °C with increasing pressure range.

85%, respectively.

GO as a stabilizing agent was recently studied for aqueous foams. GO dispersion can act as a surfactant besides AOS in the base fluid. GO has shown a significant enhancement in the thermal stability of AOS foams. The half-life of GO foams at 100 °C, and 0.69 MPa was recorded at 65 min, which increased to 190 min when the pressure increased to 6.9 MPa. Compared to AOS-only foams, the half-life was observed to increase by 150% and 220% at 0.69 MPa and 6.9 MPa, respectively. At a high temperature of 200 °C, the half-life increased from ~ 1 min to 17 min when pressure increased from 100 to 6.9 MPa. Again, at 200 °C, when compared to only AOS foams, the half-life was increased by 80% and 150% at 0.69 MPa and 6.9 MPa, respectively.

Based on the laboratory experiment results on foam stability, it was observed that foam half-life decreased with an increase in temperature. On the other hand, foam half-life increased with an increase in pressure. Moreover, stabilizing agents played a vital role in enhancing foam stability. In the past, no research studies have investigated the physical phenomena that affect foam stability under the confined conditions of temperature and pressure. It is crucial to analyze the effect of temperature and pressure on foam stability/foam half-life. The experimental data shows robust evidence of the influence of temperature; increasing temperature decreases foam half-life, while pressure positively affects foam half-life. Most of the literature research is a publication of foam half-life data based only on temperatures below 150 °C. In contrast, this research investigates the foam half-life data with the combined effect of temperature (above 150 °C) and pressure and describes the physical phenomena in foam stability based on the analytical model. In general, there is a strong relation between foam half-life with temperature and pressure that needs to be analyzed to provide guidelines for the design of stable foams to predict their behavior under given temperature and pressure.

#### 4. Discussion - analytical model

Based on the laboratory experiment results on foam stability, it was observed that foam half-life decreased with an increase in temperature. On the other hand, foam half-life increased with an increase in pressure. Moreover, stabilizing agents played a vital role in enhancing foam stability. Among all the surfactants, AOS foams showed good thermal stability performance even at high temperatures; thus, AOS foams, along with different stabilizing agents, were considered a good candidate for the analytical analysis of foam stability.

In the past, no research studies have investigated the physical phenomena that affect foam stability under the confined conditions of temperature and pressure. It is crucial to analyze the effect of temperature and pressure on foam stability/foam half-life. The experimental data shows robust evidence of the influence of temperature; increasing temperature decreases foam half-life, while pressure positively affects foam half-life. Most of the literature research is a publication of foam half-life data based only on temperatures below 150 °C. In general, there is a strong relation between foam half-life with temperature and pressure that needs to be analyzed to provide guidelines for the design of stable foams to predict their behavior under given temperature and pressure.

Modeling the effect of external variables such as temperature and pressure as a function of foam half-life would require making various assumptions considering the uniform foam system. However, there is no research on the quantitative relationship between foam half-life with temperature and pressure that can predict foam behavior and closely resembles downhole geothermal conditions. In this study, foam half-life was evaluated as a function of temperature with three significant assumptions of foam properties and structure.

**1 Mechanism of foam stability:** Foams are assumed as a colloidal system with a dispersed phase as gaseous and a continuous phase as the liquid. Most liquid foams are not stable for a very long time. Usually,

they collapse by the rupture of exposed films. Many other factors can also be identified for this, singly or in combination. Evaporation may reduce the film thickness, the surfactant concentration may be inadequate, dust may impact the films, or impurities of additives may promote their instability. Moreover, three significant phenomena that lead to foam instability are coarsening, coalescence, and drainage. Coarsening is the process of gas diffusion between foam bubbles through the thin film separating them. Coalescence is the rupture of bubble films. The downward flow of liquid through lamella borders is also known as drainage. The phenomena of coarsening and coalescence can be controlled by liquid foam drainage. Thus among all three phenomena, liquid drainage is an essential factor in considering foam stability, which is a large subject of great practical importance. Foam drainage is observed under gravity through plateau borders and lamella of liquid foams. Under this assumption, most foam drainage occurs through the plateau border, where the liquid is confined to flow down through the network of uniform and straight concave channels, also known as lamella borders. Almost no water is present at the surface of the gas bubbles of the foam structure, where foam drainage is negligible. Thus, it is assumed that foam instability is affected due to liquid drainage through the lamella border.

**2 The foam drainage mechanism is in equilibrium throughout the foam volume:** These chemical reactions are related to the gaseous phase, surfactants in the liquid film of the foams, internal pressure of foam bubbles, surface tension between foam bubbles, foam film elasticity, and foam viscosity. All these chemical reactions ultimately result in foam drainage. Foam drainage is one of the primary reactions which irreversibly evolve. Foams drain, coarsen, and finally collapse as the film between bubble ruptures due to interfacial forces involved in foam drainage and stability. Interfacial forces that arise in foam films confined between gas bubbles are critical to better understanding drainage properties and stability. Numerous theoretical and experimental data indicate that the thermodynamics and kinetic properties of liquid in thin films differ significantly from the properties of the bulk phase of the same foam solution (Park, 2014), (Abdelgawad, 2022). The complexity of fluid flow and bubble geometry has been observed in many experiments. Conceptually, the macroscopic observation of liquid drainage of foam is most simple. Experimentally, the volume or height of the liquid drained with time can be measured, but this requires a steady and reproducible initial state (Carn et al., 2009). Thus, a foam system must be uniform with a constant liquid fraction all along with its height. Such conditions are not easy to produce, especially for a high liquid fraction. For this study, foam drainage is assumed to be a uniform phenomenon that occurs throughout the volume of the foam system.

**3 Foam drainage follows first-order kinetics:** A first-order reaction is a reaction that proceeds at a rate that depends linearly on only one reactant concentration. Assuming foam drainage follows first-order kinetic reaction, under this assumption, the rate of reaction is interpreted as foam stability/foam half-life ( $t_{1/2}$ ). Moreover, the reaction occurs when liquid foam drainage through lamella borders. First-order kinetics of foam drainage can be further understood as the rate of foam volume decay at a given time is proportional to the existing foam volume for a given concentration of surfactant/stabilizing agent or foam rheological property. Thus, based on this assumption of first-order kinetics, it is understood that foam stability is directly proportional to the volume of liquid drained ( $A$ ) through the lamella borders of a foam system which can mathematically evaluate the foam half-life;

$$t_{1/2} \sim A \quad (1)$$

$$t_{1/2} = k(A) \quad (2)$$

where,

$$t_{1/2} = \text{Foam half-life}$$

$k$  = Rate constant

$A$  = Volume of liquid present in the lamella border/volume of liquid drained

Foam half-life is the time it takes for 50% of the liquid volume to drain. Foam is created when surfactant with air bubbles is inserted into a liquid. Foam half-life is described as the ratio of rate change in volume of liquid drained ( $A$ ) to change in time ( $\Delta t$ ), which is expressed as

$$t_{1/2} = \frac{-\Delta A}{\Delta t} \quad (3)$$

Thus, first order kinetics can be assumed to derive relation for foam half-life in terms of rate constant ( $k$ ). The rate constant is a proportionality constant that can express relationship between the rate of foam drainage with respect to external parameters such as temperature and pressure. To evaluate foam half-life in terms of rate constant ( $k$ ), we can equate Eq. (2) and Eq. 3;

$$k(A) = \frac{-\Delta A}{\Delta t} \quad (4)$$

Taking natural log and integration for Eq. (4), we get;

$$\ln[A]_t = -kt + \ln[A]_0 \quad (5)$$

Natural log of concentration of  $A$  at time  $t$  is equal to  $-kt$ ,  $k$  is rate constant at time  $t$  plus natural log of initial concentration of  $A$ . Graphically, natural log of  $A$  decreases with respect to time, the slope represents rate constant  $k$ . Furthermore, Eq. (5) can be solved for  $k$  as;

$$\ln[A]_t - \ln[A]_0 = -kt \quad (6)$$

$$\ln \frac{[A]_t}{[A]_0} = -kt$$

$$\frac{[A]_t}{[A]_0} = e^{-kt} \quad (7)$$

$$[A]_t = [A]_0 e^{-kt}$$

Here, when  $t = 0$ , initial concentration will be  $[A]_0$ , and at  $t = \infty$ , the foam will collapse and there is no reaction between the surfactant/stabilizing agents. To evaluate the half-life of foams, i.e.,  $t = t_{1/2}$ , initial concentration of foam surfactant will be  $\frac{[A]_0}{2}$ , thus Eq. (7) can be expressed in terms of foam half-life as;

$$\frac{[A]_0}{2} = [A]_0 e^{-kt_{1/2}}$$

$$\frac{1}{2} = e^{-kt_{1/2}}$$

Taking natural log on both the side we get;

$$\ln \left( \frac{1}{2} \right) = \ln \left( e^{-kt_{1/2}} \right)$$

$$\ln \left( \frac{1}{2} \right) = -kt_{1/2}$$

Thus,

$$t_{1/2} = \frac{0.693}{k} \quad (8)$$

This shows that, foam half-life is independent of volume of liquid drained  $A$ , its dependency has been neglected by implementing the empirical model with fitting parameters that are determined based on the experiments.

The individual effect of temperature and pressure on foam half-life was analyzed as non-linear curve fitting models described in detail in

the following sections. These models will help predict the model's fitting parameters, which can be interpreted as the physicality of foam rheological properties. As part of these individual analytical models, a comprehensive analytical model that simultaneously accounts for the effects of temperature and pressure on foam half-life will be pursued, and its relationship with the physical phenomena will be explored. Achieved through non-linear surface fitting models with two independent variables (temperature and pressure) and one dependent variable (half-life) that could help predict foam half-life at downhole conditions of high temperature and high pressure for EGS application.

#### 4.1. Foam half-life as a function of temperature

Good thermal stability is essential for foams to be utilized as a hydrofracturing fluid in EGS reservoir stimulation applications. However, from the above results for all the surfactants and stabilizing agents, temperature negatively affects foam stability; increasing temperature decreases foam stability. A study showed that temperature has a remarkable influence on microscopic structure of foam of the surfactant solution, which showed decreases in the surface tension and bubble size with increased temperature. Macroscopic results showed that the dissipation of liquid flow only partially explains foam instability through a plateau border channel. Significant discrepancies can be explained by considering different dissipation processes related to the interface's properties and the liquid flows induced in adjoining films as liquid flows in the channel (Pitois et al., 2005). Also, analysis of foam stability showed that a stable foam is observed at room temperature while unstable at a temperature above the foam base solution critical temperature due to increased coalescence rate at high temperature (H. Wang et al., 2017). It was also reported that a significant reduction in effective air mobility was observed with an increase in temperature, which increases the rate of change in bubble size at high temperatures leading to unstable foams (Sharma et al., 1985). The poor thermal stability is also due to accelerated liquid drainage and gaseous phase diffusion. Reduced foam stability may also be due to lower viscosity of the liquid phase at a higher temperature, which results in more rapid liquid drainage and hence lower foam stability (Rio et al., 2014; Minsky and Times, 2023).

Initial analytical models were developed, showing that foam stability decreases exponentially with an increase in temperature for different surfactants. However, this study is limited to low temperature (20–40 °C) and low pressure (H. Wang et al., 2017). Another literature study at a high temperature of 200 °C and high pressure of 6.9 MPa showed that liquid drainage from foam generally follows first-order kinetics. The half-life for foam volume decay declined dramatically with increasing temperature (Maini and Ma, 1986).

To date, no study shows the effect of temperature on foam half-life as an analytical model to predict foam behavior at various increasing temperature systems. This study provides an analytical model of the effect of temperature on foam half-life by considering foam drainage follows first-order kinetics. From Eq. (8), foam half-life is inversely proportional to the rate constant of foam drainage reaction. In other words, an increase in rate constant will decrease the foam half-life. i.e., the foam will have extended life when foam drainage occurs at a low rate constant. From Eq. (8), foam half-life is inversely proportional to the rate constant ( $k$ ) of foam drainage reaction. In other words, an increase in rate constant will decrease the foam half-life. i.e., the foam will have extended life when foam drainage occurs at a low rate of constant. Evaluate foam half-life as a function of the external parameter of temperature; it can be done by considering that the rate constant can be equated to external parameter temperature as a form of the Arrhenius equation, which is expressed as in Eq. 9.

$$k = D_a e^{\frac{-E_a}{RT}} \quad (9)$$

The fitting parameters of the Arrhenius equation are defined as,

$$D_a = \text{pre-exponential coefficient (min}^{-1}\text{)}$$

$E_a$  = Activation Energy ( $J \cdot mol^{-1}$ )

$R$  = Gas constant =  $0.008314 \text{ kJ} \cdot K^{-1} \cdot mol^{-1}$

Substituting rate constant ( $k$ ) from Eq. (9) in Eq. (8), we get foam half-life as a function of temperature corresponding to Arrhenius equations.

$$(t_{1/2})_f = \frac{0.693}{D_A} e^{\frac{E_a}{RT}} \quad (10)$$

Fig. 11 shows the graphical curve fitting model for Eq. (10) with goodness of fit of 0.98, which is basically the effect of foam stability concerning an increase in temperature at injection pressure of 6.9 MPa, where the half-life of foam exponentially decreases at elevated temperature following the modified Arrhenius equation.

As previously discussed, foam stability is dependent on three significant physical phenomena, coarsening, coalescence, and drainage, which leads to film rupture and decay of foam. It is studied that film rupture always occurs in the thinnest part of the lamella, where the released surface energy (Messaadi et al., 2015). The activation energy ( $E_a$ ) in Eq. (10) can be interpreted as the energy foam bubbles need to initiate drainage. In other words, the internal energy of liquid flow between the lamella borders is significantly related to the bubble film thickness and surface tension. One study verified this relation, which shows that smaller bubbles tend to produce long-lasting foam. This is because foam bubbles with a small diameter would have high surface tension, which needs a large amount of energy to break the barrier (surface tension) between foam bubbles, ultimately leading to foam collapse. The other fitting parameter in Eq. (8) is the pre-exponential coefficient which is defined as the drainage rate constant ( $D_A$ ) of foam. The fitting parameter is the rate at which the liquid flows downwards through the lamella borders of the foams due to gravity during foam collapse. It is dependent on the nature of the liquid/foam base solution, such as the type of surfactant, stabilizing agents, and rheological properties of foams, such as viscosity and bubble surface tension.

These interpretations of foams activation energy ( $E_a$ ) and drainage rate constant ( $D_A$ ) are further evaluated by taking the natural logarithm of Eq. (10).

$$\ln t_{1/2} = \ln \frac{1}{D_A} - 0.366 + \frac{E_a}{RT} \quad (11)$$

Eq. (9) resembles a linear model, which is graphically expressed by plotting  $\ln t_{1/2}$  with  $1/T$  as shown in Fig. 12. This linear model yields a straight line with a slope of  $-\frac{E_a}{R}$  and a y-intercept of  $\ln \left( \frac{1}{D_A} \right) - 0.366$ . Fig. 12 shows some examples of the linear dependence of the model to evaluate activation energy and drainage rate constant for AOS foam at different pressure ranges.

From Fig. 12, a negative slope is observed with negative activation energy, representing that with increase in temperature the rate of reaction will also increase, i.e., rapid foam drainage. Thus, the higher the  $E_a$ , the slower will be the foam drainage which is observed by an increase in foam half-life. The resulting  $E_a$  represents the energy required to initiate foam drainage at given temperature for that selected foam system. This activation energy of foam can be understood as an internal energy barrier that is controlled by its rheological properties such as foam density, viscosity, bubble diameter, bubble surface tension, and internal bubble pressure. When the foam overcomes the internal energy barrier (activation energy) due to external parameters such as temperature and pressure, the foam starts to collapse following liquid drainage. The activation energy ( $E_a$ ) and drainage rate constant ( $D_A$ ) of AOS foams were calculated by using Eq. (11) and are listed in Table 4.1 for pressure range of 0.69 MPa (0.6 MPa), 1.38 MPa (1.3 MPa), 2.07 MPa (2 MPa), 3.45 MPa (3.5 MPa), 4.14 MPa (4 MPa), 5.52 MPa (5.5 MPa), and 6.9 MPa (6.9 MPa). The negative values of the activation energies indicate that foam drainage will occur naturally due to gravity.

#### 4.1.1. Effect of stabilizing agents on activation energy ( $E_a$ ) and drainage rate ( $D_A$ ) of foams

It is crucial to analyze a pattern of activation energy and drainage rate concerning different stabilizing agents and at constant pressure. This can give further insight into how these parameters are affected by controlling pressure and stabilizing agents under the influence of temperature. This section focuses on the effect of different stabilizing agents.

Graphical plots were modeled representing the activation energy for AOS foams with different stabilizing agents for a pressure ranging from 0.6 MPa to 6.9 MPa as seen in Fig. 13. It is noticed that addition of the stabilizing agents does not give a subsequent trend for  $E_a$ ; however, AOS foams with addition of stabilizing have mean activation energy at each pressure range. For example, the  $E_a$  for AOS foams with stabilizing agents were  $-50.68 \text{ kJ/mol}$ ,  $-40.41 \text{ kJ/mol}$ , and  $-32.98 \text{ kJ/mol}$  at 0.6 MPa, 3.5 MPa, and 6.9 MPa, respectively.

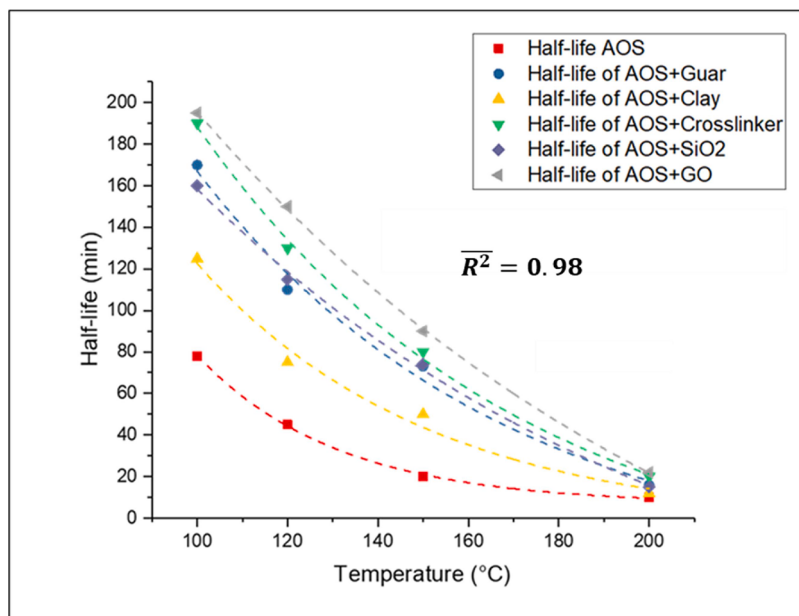


Fig. 11. Modified Arrhenius exponential decay curve fitting model of temperature effect on foam half-life at 6.9 MPa.

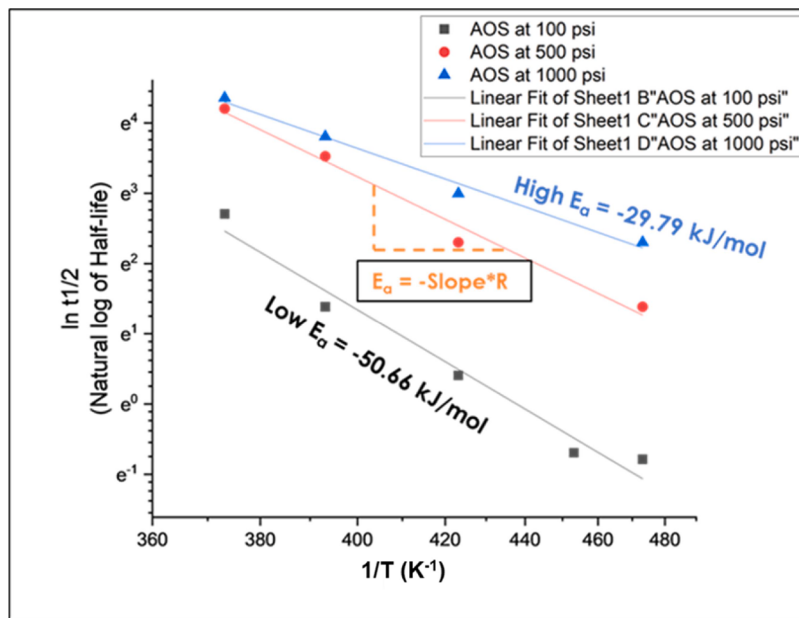


Fig. 12. Linear log model for AOS foams at different pressure range to evaluate activation energy.

Table 4.1

Activation energy and drainage rate of AOS foams at different pressure.

Foam Composition	0.69 MPa $D_A$ (min <sup>-1</sup> )	$E_a$ (kJ/mol)	R <sup>2</sup>	1.38 MPa $D_A$ (min <sup>-1</sup> )	$E_a$ (kJ/mol)	R <sup>2</sup>	2.07 MPa $D_A$ (min <sup>-1</sup> )	$E_a$ (kJ/mol)	R <sup>2</sup>
AOS	1.0E+6	-50.63	0.96	6.8E+4	-44.50	0.90	4.9E+4	-45.03	0.95
AOS+Guar	3.0E+5	-48.67	0.98	3.8E+4	-44.53	0.95	4.8E+4	-47.13	0.96
AOS+Clay	6.0E+5	-50.95	0.97	5.0E+4	-44.55	0.98	2.3E+5	-45.05	0.99
AOS+Crosslinker	8.2E+5	-53.67	0.90	2.6E+4	-44.38	0.92	2.6E+4	-45.71	0.95
AOS+SiO <sub>2</sub>	2.0E+5	-48.71	0.92	1.0E+5	-48.75	0.93	3.7E+4	-46.41	0.97
AOS+GO	4.5E+5	-52.34	0.92	3.0E+4	-45.35	0.93	1.1E+4	-43.21	0.92
Foam Composition	3.45 MPa $D_A$ (min <sup>-1</sup> )	$E_a$ (kJ/mol)	R <sup>2</sup>		4.14 MPa $D_A$ (min <sup>-1</sup> )	$E_a$ (kJ/mol)	R <sup>2</sup>		
AOS	9.1E+3	-41.38	0.97		1.8E+3	-36.54	0.95		
AOS+Guar	2.5E+4	-46.40	0.88		9.9E+3	-44.25	0.99		
AOS+Clay	1.6E+3	-36.51	0.95		4.5E+2	-33.02	0.96		
AOS+Crosslinker	3.9E+3	-41.09	0.92		2.5E+3	-40.28	0.97		
AOS+SiO <sub>2</sub>	1.9E+3	-39.61	0.95		1.7E+3	-39.03	0.97		
AOS+GO	1.8E+3	-38.70	0.98		1.8E+3	-39.79	0.92		
Foam Composition	5.52 MPa $D_A$ (min <sup>-1</sup> )	$E_a$ (kJ/mol)	R <sup>2</sup>		6.9 MPa $D_A$ (min <sup>-1</sup> )	$E_a$ (kJ/mol)	R <sup>2</sup>		
AOS	2.0E+2	-29.98	0.98		1.7E+2	-29.79	0.98		
AOS+Guar	1.7E+3	-39.25	0.97		3.3E+2	-34.64	0.96		
AOS+Clay	2.2E+2	-31.55	0.99		2.0E+2	-31.85	0.97		
AOS+Crosslinker	6.7E+2	-36.81	0.98		1.8E+2	-33.31	0.90		
AOS+SiO <sub>2</sub>	3.9E+2	-34.84	0.94		2.1E+2	-33.55	0.91		
AOS+GO	7.9E+2	-37.80	0.91		2.5E+2	-34.74	0.94		

From Table 4.1, it is observed that drainage rate ( $D_A$ ) drastically decreases with the addition of all stabilizing agents in comparison with only AOS as surfactants. This is explained in terms of a decrease in liquid drainage through the lamella border with the addition of stabilizing agents, as each stabilizing agent has a unique effect on the foam base fluid rheological properties, particularly its viscosity highly influences the foam drainage.

It is known that increased viscosity will reduce foam drainage (Azdarpour et al., 2013; Farajzadeh et al., 2008) as it is challenging to drain the high viscous liquid through foam lamella borders. Other factors such as foam bubble surface tension also play a critical role in determining the  $D_A$ , which is far more complex to illustrate as it will need to understand the pressure difference between foam bubbles.

From Fig. 13, it is comprehensible that with the addition of

stabilizing agents, there is no significant trend observed but average activation energy. On the other hand, it is also observed that with an increase in pressure, the  $D_A$  value decreases for AOS foams and AOS foams with stabilizing agents; this is the effect of pressure on drainage rate that is explored in detail in the next section.

#### 4.1.2. Effect of pressure on drainage rate ( $D_A$ ) and activation energy ( $E_a$ ) of foams

The drainage rate constant ( $D_A$ ) and activation energy ( $E_a$ ) are highly influenced by pressure. Drainage rate is understood as the rate of liquid flowing through the lamella border of foam bubbles. Fig. 14 illustrates a logarithm decrease of  $D_A$  with an increase in pressure for all AOS foams with stabilizing agents. The  $D_A$  is influenced by several rheological properties of foam bubbles, much likely by bubble surface tension, foam

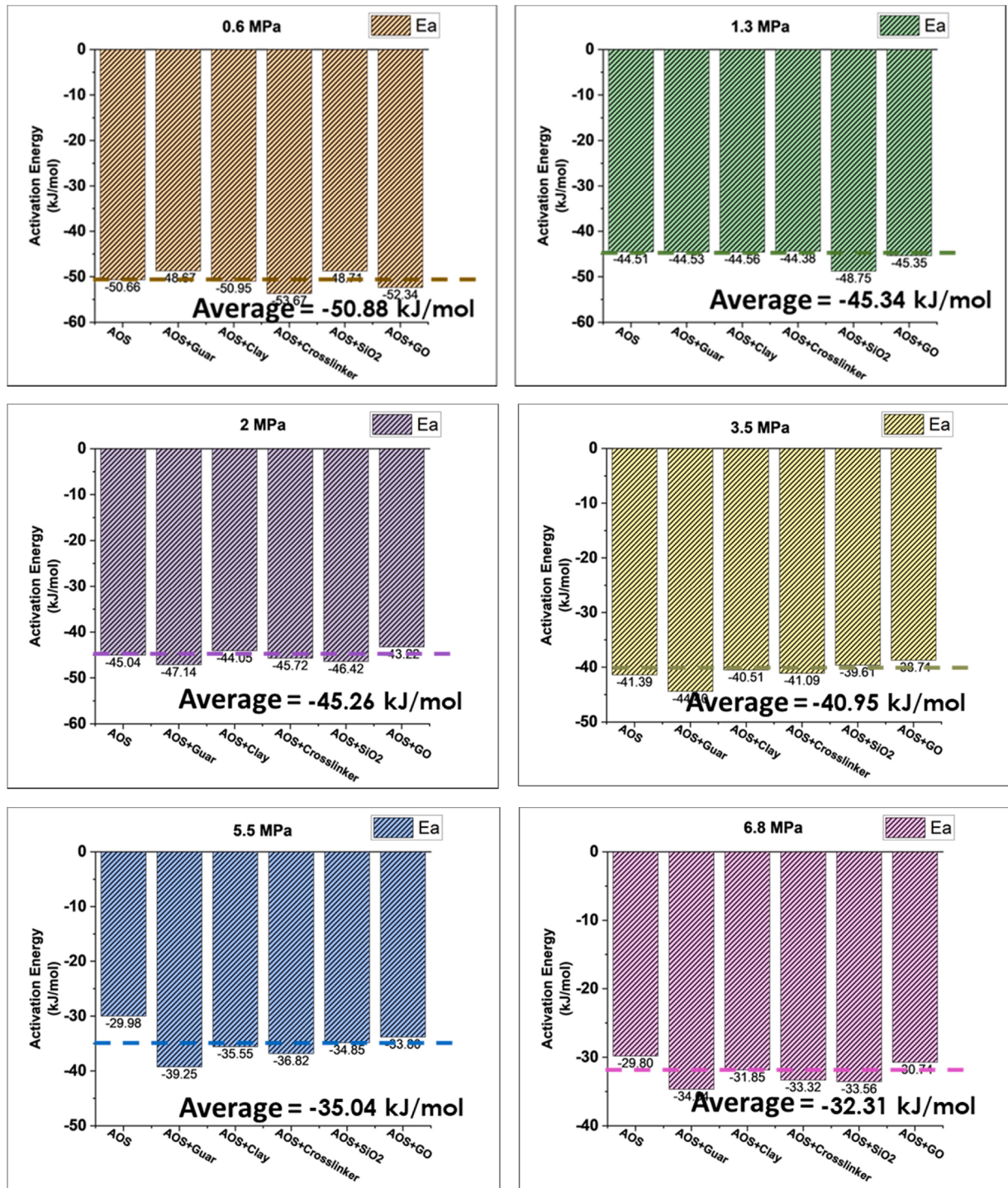


Fig. 13. Effect of stabilizing agents on activation energy ( $E_a$ ) for AOS foams.

bubble size, and foam bubble internal pressure, which are all closely related to the injection pressure. Several works of literature explained that the stability of bubbles concerning elevated pressure leads to smaller bubble sizes and narrow bubble size distributions. Moreover, foam bubble stability at high pressure is significantly higher due to high gas inertia and low gas-liquid surface tension (Piskulich et al., 2019). This decrease in bubble size showed increased foam stability, which resulted in a slower drainage rate at high pressure.

A semi-logarithmic plot is used to perceive a relationship between  $D_A$  and pressure. Fig. 14 plot is useful to visualize large values of  $D_A$  on y-axis as a log scale with pressure on x-axis as linear scale.

The pressure dependence of  $D_A$  can be described as

$$\ln(D_A) = mP + b \quad (12)$$

where  $m$  and  $b$  are fitting parameters, which represent the slope and the y-intercept of the fitted curve, respectively. The values of the fitting parameters are listed Table 4.2.

From Fig. 15, the trend observed for activation energy is that with increased pressure, the activation energy is increased for all the AOS foams with stabilizing agents. The activation energy of each foam with the stabilizing agent has its mean activation energy where the foam starts to drain beyond that energy barrier. This energy barrier increases

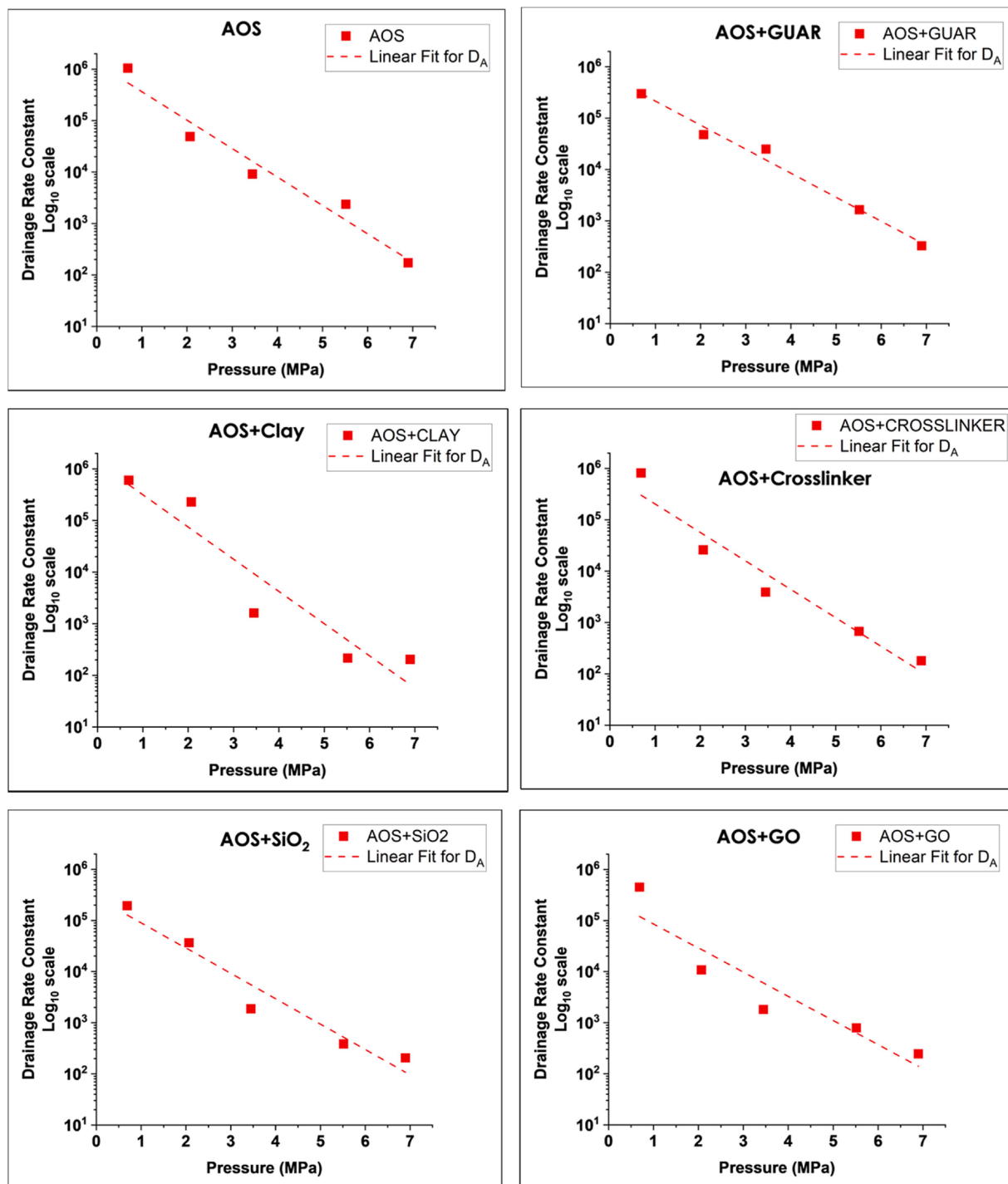


Fig. 14. Effect of pressure on drainage rate constant ( $D_A$ ) of foams.

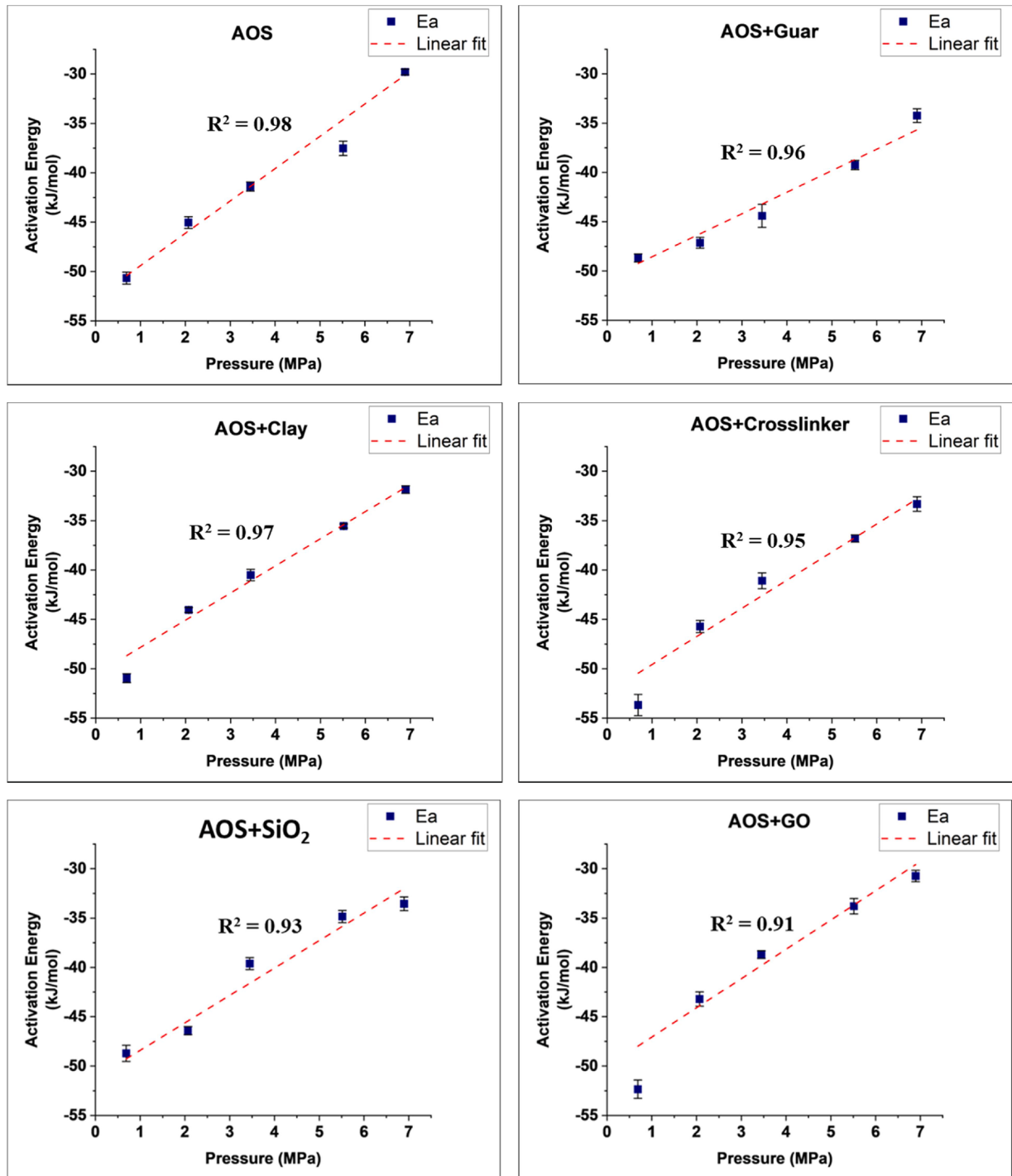
Table 4.2

Fitting parameters for Eq. (10),  $D_A$  is logarithmically dependent on pressure.

Foam Composition	b (min <sup>-1</sup> )	m (MPa <sup>-1</sup> )
AOS	6.11	-0.55
AOS+GUAR	5.80	-0.46
AOS+CLAY	6.12	-0.62
AOS+CROSSLINKER	5.86	-0.55
AOS+SiO <sub>2</sub>	5.45	-0.49
AOS+GO	5.41	-0.47

with an increase in pressure. The decay of the AOS foam structure under the influence of external pressure will show increase in surface tension which take long time for coarsening. The activation energy is -50.63 kJ/mol at 0.6 MPa and compared with that at 6.9 MPa, which is -29.79 kJ/mol here, so we can see that foams with higher activation energy takes more time to decompose. Moreover, it's also observed that, a high activation energy is achieved with increase in pressure. Similarly, all the AOS foams with stabilizing agents showed the same positive effect for activation energy, where an increase in pressure showed an increase in activation energy and long-lasting foams.

A linear relationship between activation energy and pressure was

Fig. 15. Effect of pressure on activation energy ( $E_a$ ) of foams.

observed, as shown in Eq. (13),

$$E_a = V_m P + E'_a \quad (13)$$

where,  $V_m$  is the molar volume and  $E'_a$  is the total energy. The physical meanings of these parameters will be discussed in the next section. It can be understood that higher  $E_a$  has a steeper slope which resembles sensitivity to change in pressure and low  $E_a$  is less sensitive to pressure change. Increase in pressure, a significant increase in activation energy is observed as linear relation. Table 4.3 shows an example of linear fitting to Eq. (13).

**Table 4.3**  
Fitting parameters for liner fit model of effect of pressure on activation energy.

Foam Composition	Slope ( $m$ ) (kJ/(mol. MPa))	Intercept ( $c$ ) (kJ/mol)
AOS	3.27	-52.67
AOS+Guar	2.18	-50.74
AOS+Clay	2.75	-50.56
AOS+Crosslinker	2.84	-52.40
AOS+SiO <sub>2</sub>	2.78	-51.19
AOS+GO	2.97	-50.03

## 5. Effect of temperature and pressure

No literature study has evaluated the combined effect of temperature and pressure on foam stability. This research indicates that with an optimum selection of surfactants and stabilizing agents, it is viable to obtain stable foams as potential fracturing fluid at the downhole condition for EGS application that is high temperature fracturing of HDR and high-pressure injection of fracturing fluid. The combined effect of temperature and pressure develops a unified model for foam stability. The temperature negatively impacts foam half-life (increase in temperature foam half-life decreases); on the other hand, pressure appears to positively affect foam half-life (increase in pressure foam half-life increases). The temperature effect on foam half-life from Eq. (10) is modified to develop the unified foam stability model.

Based on Eq. (13), it corresponds to a linear equation with fitting parameters  $V_m$  and the slope and  $E_a'$  as the intercept of the fitting model. Furthermore, applying dimensionless analysis to Eq. (13), the slope,  $V_m$  has unit of  $(\frac{kJ}{MPa.mol})$  and intercept  $E_a'$  has a unit of  $kJ/mol$ , which is same as the activation energy of foams or total free energy of foams. The slope fitting parameter ( $V_m$ )'s base unit's physical significance is analyzed and tracked. From the dimensionless analysis of Eq. (13), it is known that the base unit of  $V_m$  is analyzed as  $(\frac{kJ}{MPa.mol})$  which can also be simplified as,

$$V_m = \frac{kJ}{MPa.mol} \Rightarrow \frac{kJ}{MPa} \Rightarrow \frac{J}{Pa} = m^3$$

Also,

$$V_m = \frac{kJ}{MPa.mol} = \frac{\frac{10^3 kgm^3}{s^2}}{\frac{10^6 kg}{ms^2.mol}} = \frac{m^3}{10^3.mol} = \frac{10^{-3} m^3}{mol} = \frac{dm^3}{mol}$$

Thus,  $V_m$  has a typical unit of molar volume of gas. The molar volume of gas in foams can be interpreted as the volume of gas in the foam at a given temperature and pressure. It is also related to the internal energy in the pressurized foam gas bubbles that keeps the bubble from not bursting. The slope ( $V_m$ ) will represent the molar volume of the gas phase, and the intercept ( $E_a'$ ) is the free energy to initiate drainage in the foams when no pressure is applied to the system. substituting  $E_a$  to Eq. (10),

$$(t_{1/2})_f = \frac{0.693}{D_A} e^{\left( \frac{V_m P - E_a'}{RT} \right)} \quad (14)$$

The above Eq. (14) can predict foam stability under the influence of external parameters, temperature, and pressure. Figs. 16–18 show 3D non-linear surface fitting to Eq. (14) for AOS foams with different

stabilizing agents. The fittings show an average goodness of fit ( $R^2$ ) of 0.91.

It is worthwhile to make further discussion on several parameters to illustrate their influence on foam stability.

### 5.1. Drainage rate constant, $D_A$ ( $min^{-1}$ )

It is the rate at which the liquid flows downwards through the lamella borders of the foams due to gravity (Bikerman, 1973).  $D_A$  is dependent on the nature of the liquid/foam base solution, such as the type of the surfactant, stabilizing agents, and the rheological properties of foams like viscosity, bubble surface tension, internal gas pressure, and bubble diameter (Teixeira and Fortes, 2007; Lin et al., 1998). The  $D_A$  is observed to decrease with the addition of stabilizing agents;  $D_A$  of AOS foams is calculated as  $2706.87 min^{-1}$ ; however, with the addition of stabilizing agents such as GO dispersion, the drainage rate subsequently decreases to  $147.54 min^{-1}$ . Thus, it is observed that with the addition of GO dispersion, the liquid between the lamella border drainage is slower, producing long-lasting foams compared to only AOS foams.

Also, from Eq. (12),  $D_A$  is inversely proportional to foam half-life. The slower the drainage rate, the higher the foam's half-life, which will generate long-lasting foams. Drainage rate is a foam base fluid property verified by considering the inverse proportionality relation to foam half-life. Assuming  $D_A \rightarrow 0$ ,  $t_{1/2} \rightarrow \infty$ , that means the drainage is not initiated, and the system is in the liquid phase; vice versa, if  $D_A \rightarrow \infty$ ,  $t_{1/2} \rightarrow 0$ , that is the liquid from the foam system has completely drained out and there is not foam left. It is also observed that the  $D_A$  is also strongly influenced by pressure,  $D_A$  linearly decreases with increase in pressure. Since at high inject pressure, foam bubble size is relatively smaller and spherical, preventing slower gas transport between the bubbles and reducing coarsening (German et al., 2018). For stabilizing agents, it is calculated that, on average,  $D_A$  decreases by 95% with an increase in pressure from 100 to 6.9 MPa.

### 5.2. Free energy, $E_a'$ ( $kJ/mol$ )

The relation of  $E_a'$  to foam stability is encountered from the Arrhenius equation, where foam half-life is exponentially to  $E_a'$ . This relation provides adequate knowledge on foam stability energy barrier related to its rheological properties. It is expressed as the total internal energy barrier of a foam system which is highly impacted by the external parameters such as temperature and pressure rather than foam composition. It is the energy needed by the foam to initiate liquid drainage. In other words, the liquid's internal energy flows through the lamella border and completely drains out. The activation energy does not show

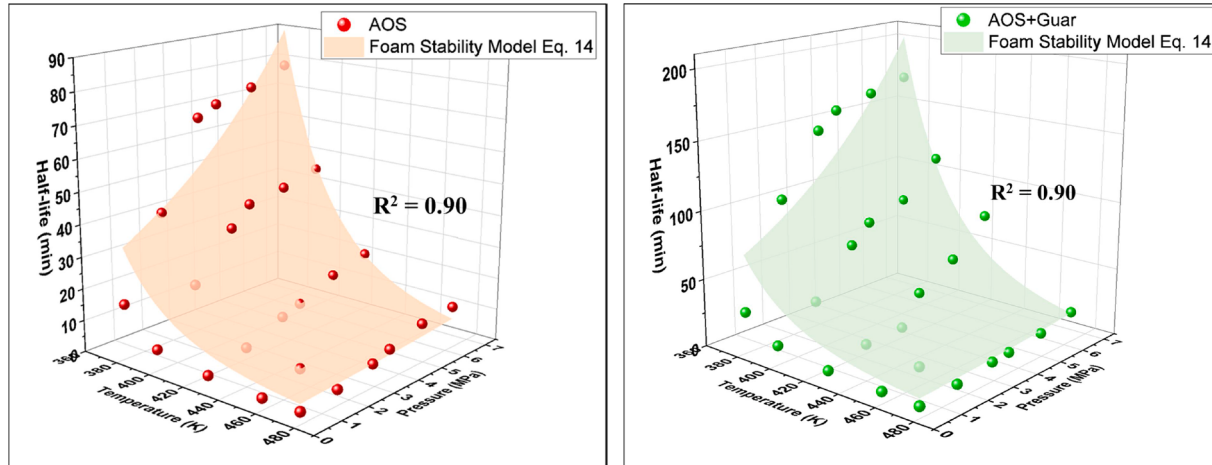


**Fig. 16.** Surface fitting to Eq. (14) for AOS (left) and AOS+Guar (right) foams showing the combined effect of temperature and pressure on foam half-life.

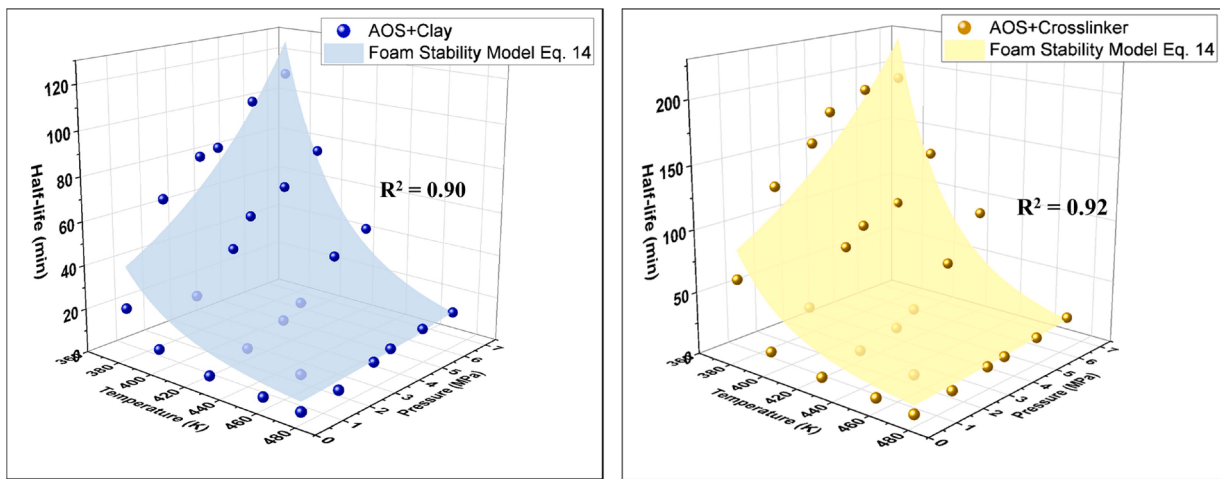


**Fig. 17.** Surface fitting to Eq. (12) for AOS+Clay (left) and AOS+Crosslinker (right) foams showing the combined effect of temperature and pressure on foam half-life.

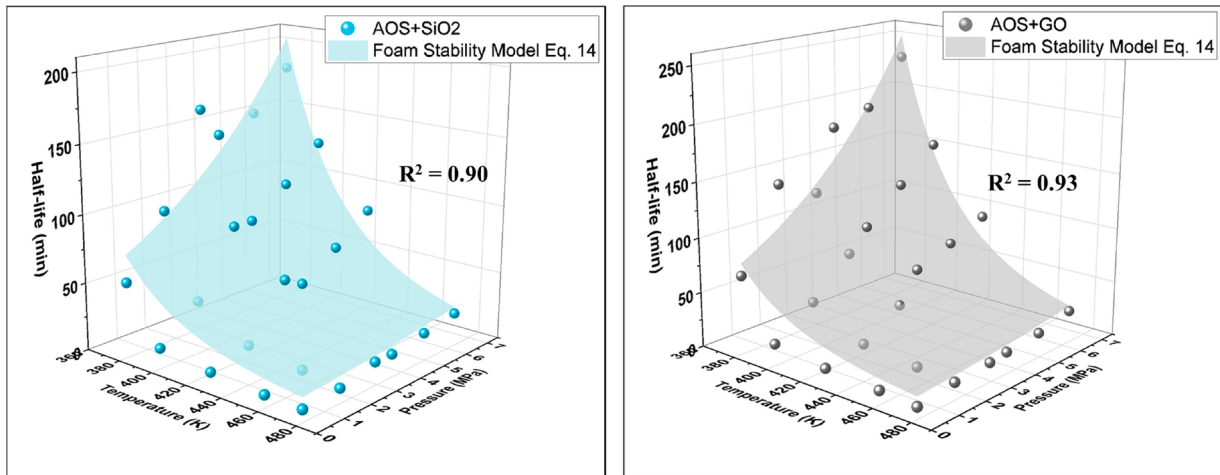


**Fig. 18.** Surface fitting to Eq. (12) for AOS+SiO<sub>2</sub> nanoparticles (left) and AOS+GO (right) foams showing the combined effect of temperature and pressure on foam half-life.

significant variation, but minor variations can be observed with the addition of stabilizing agents such as the  $E_a'$  of AOS foam calculated at  $-36.15 \text{ kJ/mol}$ , and with the addition of stabilizing agents such as SiO<sub>2</sub> nanoparticles and GO the  $E_a'$  is increased to  $-28.29 \text{ kJ/mol}$  and  $-29.66 \text{ kJ/mol}$ . Thus, with the addition of stabilizing agents, the foam's internal energy barrier increases (higher activation energy), indirectly increasing the foam's half-life as it would need higher energy from external parameters to initiate foam drainage to decay the foam. The negative value of activation energy indicates that the rate of reaction decreases with an increase in temperature, that is, the foam-half-life is decreased with increase in temperature and higher the  $E_a'$  slower will be foam drainage (Langevin, 2019; Anon 2016).  $E_a'$  is slightly dependent on the foam composition as the mean  $E_a'$  for AOS foams with stabilizing agents is  $32.43 \text{ kJ/mol}$ . In contrast, the activation energy greatly varies with an external parameter of pressure due to the pressure effect on foam stability  $E_a'$  increases with increase in injection pressure generating long lasting foams. This model will predict the energy needed by foam composition to initiate drainage under the influence of temperature and pressure.

### 5.3. Molar volume, $V_M$ (l/mol)

Molar volume is another parameter related to foam stability under the influence of external parameters such as temperature and pressure. For ideal gasses, the molar volume is defined by an ideal gas equation which can be rearranged to give an expression for the molar volume of an ideal gas  $V_m = \frac{RT}{P}$ . Hence for a given temperature and pressure, the molar volume is the same for all ideal gasses and is related to the gas constant  $R$  (Duarte, 2000). The molar volume of a gas expresses the volume occupied by 1 mole of that respective gas under specific temperature and pressure conditions. The most common example is a gas's molar volume at STP (Standard Temperature and Pressure), which is equal to  $22.4 \text{ L}$  for 1 mole of any ideal gas at a temperature of  $273.15 \text{ K}$  and a pressure of 1 atm (Zhou and Battino, 2001).

The molar volume of a gas expresses the volume occupied by 1 mole of that respective gas under specific temperature and pressure conditions. The most common example is a gas's molar volume at STP (Standard Temperature and Pressure), which is equal to  $22.4 \text{ L}$  for 1 mole of any ideal gas at a temperature of  $273.15 \text{ K}$  and a pressure of 1 atm. The  $V_M$  of different foam compositions does not vary greatly but has an average  $V_M \sim 0.5 \text{ dm}^3/\text{mol}$ . Furthermore, the  $V_M$  of foams will also provide detailed insights on the pressure in the continuous liquid phase as it is known that pressure between the gas phase and liquid phase of

the bubble is defined by  $(P_{\text{gas}} - P_{\text{liquid}}) = \frac{2T}{R}$ , where  $T$  is the surface tension of bubbles, and  $R$  is the gas constant (David and Nauze, 1972). The pressure difference between the inner gas phase and outer liquid phase is directly proportional to the surface tension and inversely proportional to the bubble's radius. The molar volume of the foam system is highly complex to analyze, related to measuring foam bubble internal pressure and surface tension.

In summary, a unified model for foam stability for temperature and pressure is developed based on the experimental half-life data recorded for a temperature range of 100 °C to 200 °C and a pressure range of 0.69 MPa to 6.9 MPa. This model can predict foam stability behavior under high pressure and high temperature. Moreover, based on the unified model of foam stability, fitting parameters are defined, calculated, and analyzed. Foam stability for a particular foam composition can be predicted under the external factor of temperature and pressure by understanding foam's physical properties, drainage rate ( $D_A$ ), total energy ( $E_a$ ) and molar volume ( $V_M$ ) can be predicted based on Eq. (12). These factors are complex to analyze as they occur at the microscale and nanoscale levels. However, they are directly related to foam composition and its rheological properties.

The calculated drainage rate, activation energy, and molar volume are based on AOS foams. It is expected that the general model (Eq. (14)) can be used on other aqueous foams. However, further investigation is needed to test this hypothesis via testing the thermal stability of foams containing other surfactants such as SDS, CATC, and NP-40. Changes in foam composition could give different values to the fitting parameters.

## 6. Conclusions

This research aims to explore thermally stable foams as hydrofracking fluid media for potential applications in the enhanced geothermal system (EGS). Throughout this project, significant effort was executed to collect data relevant to foam fracturing.

This experiment aims to evaluate thermodynamic behavior of foams at high temperature and high-pressure conditions closely resembling the geothermal environment. In this study, foam behavior was categorized as foam stability based on its half-life, i.e., the time taken by the liquid volume to drain from the foam and decrease by 50% of its original height. The Laboratory apparatus measures the foam half-life for a temperature range of 100 °C to 200 °C and a pressure range of 0.69 MPa to 6.9 MPa. Two types of dispersed/gaseous phases were investigated: nitrogen gas ( $N_2$ ) and carbon dioxide gas ( $CO_2$ ). Four different types of commercial foaming agents/surfactants with various concentrations were tested, including Alpha olefin sulfonate (AOS), Sodium dodecyl sulfonate (SDS), Tergitol™ (NP – 40), and Cetyltrimethylammonium chloride (CTAC). Moreover, five stabilizing agents, guar gum, bentonite clay, crosslinker, silicon dioxide nanoparticles ( $SiO_2$ ), and graphene oxide dispersions (GO), were also added to the surfactant to analyze foam stability.

Initial results showed that  $N_2$  foams were more stable compared to  $CO_2$  foams. It was observed that foam half-life was decreased with an increase in temperature. Among all the surfactants, AOS foams showed the most promising results in thermal stability at high temperatures. Moreover, with the addition of stabilizing agents, foam's half-life was enhanced. Stabilizing agents such as crosslinker and GO dispersion showed the most stable foams with half-life recorded at 20 min and 17 min, respectively, at 200 °C and 6.9 MPa. Temperature showed a negative effect on foam stability which was with an increase in temperature, foam stability decreased, and pressure also showed a positive effect on foam stability that is, with an increase in pressure the foam half-life was increased. Finally, pressure also showed a positive effect on foam stability; with increased pressure, foam half-life was increased.

Relations between foam half-life and different fitting parameters were analyzed and discussed. The effect of temperature on foam stability was studied as an exponential decay model, which was explained in

terms of the Arrhenius equation and activation energy. A linear relation was developed for the effect of pressure with foam activation energy which showed that an increase in pressure would increase activation energy resulting in long lasting foams. Also, with increase in pressure drainage rate decrease linearly, which resembled slower liquid movement through lamella border with increase in pressure. Foam stability and drainage rates were strongly dependent on temperature, pressure, and gas composition.

The present study attempted to address these issues by proposing a unified non-linear surface curve fitting model for predicting foam stability/half-life. Finally, a non-linear surface curve fitting model was developed to predict foam half-life from its drainage rate, total activation energy, and molar volume when under the influence of temperature and pressure.

In this work, foam properties were explored under high temperature and pressure conditions and developed an analytical model that can be used to predict foam stability as a function of temperature and pressure. This research can provide valuable information on foam stability which is critical for foam-based hydraulic fracturing. The results indicate that with an appropriate selection of surfactants and stabilizing agents, it is possible to obtain stable foams, which could replace conventional water fracturing fluid in EGS applications.

## Author statement

This research was performed as part of a PhD thesis for the author. The research and experiment were carried out at Temple University, College of Engineering. The research was carried out with collaboration of Oak Ridge National Laboratory and under the guidance of Dr. Fei Ren (advisor advising role). The research experimental setup was constructed by the author which was a state-of-the-art setup which could measure foam stability at high pressure and high temperature. This experimental results should be useful to several researchers who studies foam behavior for EGS application.

## Declaration of Competing Interest

The authors declare that they have no known competing financial interests or personal relationships that could have appeared to influence the work reported in this paper.

## Data availability

Data will be made available on request.

## Acknowledgement

This research was sponsored by the US Department of Energy, Assistant Secretary for Energy Efficiency and Renewable Energy, Geothermal Technologies Office, as part of the Enhanced Geothermal Systems Program under Contract No. DE-AC05-00OR22725 with the US Department of Energy.

## References

- Lu, S.M., 2018. A global review of enhanced geothermal system (EGS). Renew. Sustain. Energy Rev. 81 (June 2017), 2902–2921. <https://doi.org/10.1016/j.rser.2017.06.097>.
- Gaurina-Medimurec, N., Brkić, V., Topolovec, M., Mijić, P., 2021. Fracturing fluids and their application in the Republic of Croatia. Appl. Sci. 11 (6) <https://doi.org/10.3390/app11062807>.
- Barati, R., Liang, J.T., 2014. A review of fracturing fluid systems used for hydraulic fracturing of oil and gas wells. J. Appl. Polym. Sci. 131 (16) <https://doi.org/10.1002/app.40735>.
- Huang, Z., 2018. New Fracturing Fluids and Fracturing Methods Nuclear Magnetic Resonance Theories.

- Olasolo, P., Juárez, M.C., Morales, M.P., Damico, S., Liarte, I.A., 2016. Enhanced geothermal systems (EGS): a review. *Renew. Sustain. Energy Rev.* 56, 133–144. <https://doi.org/10.1016/j.rser.2015.11.031>.
- Reber, T.J., Beckers, K.F., Tester, J.W., 2014. The transformative potential of geothermal heating in the U.S. energy market: a regional study of New York and Pennsylvania. *Energy Policy* 70, 30–44. <https://doi.org/10.1016/j.enpol.2014.03.004>.
- Clark, C.E., Harto, C.B., Sullivan, J.L., Wang, M.Q., 2010. Water use in the development and operation of geothermal power plants. *Energy Syst. Div. Argonne Natl. Lab.* (January), 1–87. <https://doi.org/10.2172/1013997>.
- Kohshou, L.O., et al., 2017. Economic assessment and review of waterless fracturing technologies in shale resource development: a case study. *J. Earth Sci.* 28 (October 2017), 933–948.
- Mordis and George, "Literature review and analysis of waterless fracturing methods," 2017.
- Gandossi, L., 2016. State of the Art Report on Waterless Stimulation Techniques for Shale Formations.
- Wang, H., Wang, J.J., Polsky, Y., Ren, F., Thakore, V., 2019. Research considerations for foam fracturing in stimulation development for enhanced geothermal systems. In: 44th Workshop on Geothermal Reservoir Engineering, pp. 1–11 [Online]. Available. <https://www.semanticscholar.org/paper/Considerations-for-Foam-Fracturing-in-Stimulation-Wang-Wang-f33ea2cbad8c2a192a782cd8ffd88689adeab8d5f>.
- Wanniarachchi, W.A.M., Ranjith, P.G., Perera, M.S.A., 2017. Shale gas fracturing using foam-based fracturing fluid: a review. *Environ. Earth Sci.* 76 (2), 1–15. <https://doi.org/10.1007/s12665-017-6399-x>.
- Frohne, H., 1976. Comparison of conventional hydraulic and water/nitrogen foam fracturing in two Ohio Devonian shale gas wells. *Pap. Knowl. Towar. a Media Hist. Doc.* (February), 12–26.
- Riedel, E.F., 1981. An assessment of environmental health and safety issues associated with the commercialization of unconventional gas recovery: Huron shale. *PNL Rep 148*, 148–162.
- Wanniarachchi, W.A.M., Ranjith, P.G., Perera, M.S.A., Lashin, A., Al Arifi, N., Li, J.C., 2015. Current opinions on foam-based hydro-fracturing in deep geological reservoirs. *Geomech. Geophys. Geo-Energy Geo-Resources* 1 (3–4), 121–134. <https://doi.org/10.1007/s04948-015-0015-x>.
- Oussoltsev, D., et al., 2008. Foam fracturing: new stimulation edge in Western Siberia. *Soc. Pet. Eng. - SPE Russ. Oil Gas Tech. Conf. Exhib.* 2008 1, 636–648. <https://doi.org/10.2118/115558-ms>.
- Yekken, N., Padmanabhan, E., Idris, A.K., 2018. A review of recent advances in foam-based fracturing fluid application in unconventional reservoirs. *J. Ind. Eng. Chem.* 66, 45–71. <https://doi.org/10.1016/j.jiec.2018.05.039>.
- Wang, H., Wang, J.J., Polsky, Y., Ren, F., Thakore, V., 2021. Study on foam fracturing of granite for the development of enhanced geothermal systems a. In: 46th Workshop on Geothermal Reservoir Engineering, pp. 348–360.
- Wilk, K., 2019. Experimental and simulation studies of energized fracturing fluid efficiency in tight gas formations. *Energies* 12 (23). <https://doi.org/10.3390/en12234465>.
- Lai, C.Y., Rallabandi, B., Perazzo, A., Zheng, Z., Smiddy, S.E., Stone, H.A., 2018. Foam-driven fracture. *Proc. Natl. Acad. Sci. U. S. A.* 115 (32), 8082–8086. <https://doi.org/10.1073/pnas.1808068115>.
- Faroughi, S.A., Pruvot, A.J.C.J., McAndrew, J., 2018. The rheological behavior of energized fluids and foams with application to hydraulic fracturing: review. *J. Pet. Sci. Eng.* 163 (July 2017), 243–263. <https://doi.org/10.1016/j.petrol.2017.12.051>.
- Thomas, G.L., 2015. Wet foam coarsening evidence a self similar growth regime. *Physiol. Behav.* 176 (12), 139–148. <https://doi.org/10.1016/j.colsurfa.2015.02.0153D>.
- Georgieva, D., Cagna, A., Langevin, D., 2009. Link between surface elasticity and foam stability. *Soft Matter* 5 (10), 2063–2071. <https://doi.org/10.1039/b822568k>.
- Saint-Jalmes, A., 2006. Physical chemistry in foam drainage and coarsening. *Soft Matter* 2 (10), 836–849. <https://doi.org/10.1039/b606780h>.
- Wang, H., Guo, W., Zheng, C., Wang, D., Zhan, H., 2017a. Effect of temperature on foaming ability and foam stability of typical surfactants used for foaming agent. *J. Surfactants Deterg.* 20 (3), 615–622. <https://doi.org/10.1007/s11743-017-1953-9>.
- Wang, Y., et al., 2017b. The stability study of CO<sub>2</sub> foams at high pressure and high temperature. *J. Pet. Sci. Eng.* 154 (April), 234–243. <https://doi.org/10.1016/j.petrol.2017.04.029>.
- P.B. Rand and O.J. Montoya, "Evaluation of aqueous-foam surfactants for geothermal -drilling fluids," pp. 1–28, 1983, [Online]. Available: <https://www.osti.gov/servlets/purl/5623483>.
- Thakore, V., et al., 2020. High-temperature stability of aqueous foams as potential waterless hydrofracking fluid for geothermal reservoir stimulation. In: PROCEEDINGS, 44th Work. Geotherm. Reserv. Eng. Stanford Univ. Stanford, California, Febr. 10–12, 2020 SGP-TR-216, pp. 1–10.
- Ahmed, S., Elraies, K.A., Hashmet, M.R., Alnarabiji, M.S., 2018. Empirical modeling of the viscosity of supercritical carbon dioxide foam fracturing fluid under different downhole conditions. *Energy* 11 (4). <https://doi.org/10.3390/en11040782>.
- Chen, Y., et al., 2014. Switchable nonionic to cationic ethoxylated amine surfactants for CO<sub>2</sub> enhanced oil recovery in high-temperature, high-salinity carbonate reservoirs. *SPE J* 19 (2), 249–259. <https://doi.org/10.2118/154222-PA>.
- Chen, Y., et al., 2016. High temperature CO<sub>2</sub>-in-water foams stabilized with cationic quaternary ammonium surfactants. *J. Chem. Eng. Data* 61 (8), 2761–2770. <https://doi.org/10.1021/acs.jced.6b00135>.
- Harris, P.C., Reidenbach, V.G., 1987. High-Temperature Rheological Study of Foam Fracturing Fluids. *JPT. J. Pet. Technol.* 39 (5), 613–619. <https://doi.org/10.2118/13177-PA>.
- Harris, P.C., 1993. Chemistry and rheology of borate-crosslinked fluids at temperatures to 300°F," *JPT. J. Pet. Technol.* 45 (3), 264–269. <https://doi.org/10.2118/24339-PA>.
- Miller, M., 2005. A circulating foam loop for evaluating foam at conditions of use. *SPE Prod. Facil.* 20 (4), 286–294.
- Verma, A., Chauhan, G., Ojha, K., 2017. Synergistic effects of polymer and bentonite clay on rheology and thermal stability of foam fluid developed for hydraulic fracturing. *Asia-Pacific J. Chem. Eng.* 12 (6), 872–883. <https://doi.org/10.1002/apj.2125>.
- Zhang, P., et al., 2019. Enhanced stability and high temperature-tolerance of CO<sub>2</sub> foam based on a long-chain viscoelastic surfactant for CO<sub>2</sub> foam flooding. *RSC Adv* 9 (15), 8672–8683. <https://doi.org/10.1039/c9ra00237e>.
- Thakore, V., Ren, F., Voytek, J., Wang, H., Wang, J.J., Polsky, Y., 2021. High temperature stability of aqueous foams for potential application in enhanced geothermal system (EGS). In: PROCEEDINGS, 45th Work. Geotherm. Reserv. Eng. Stanford Univ. Stanford, California, Febr. 10–12, 2021, pp. 336–347.
- Emrani, A.S., Nasr-El-Din, H.A., 2017. Stabilizing CO<sub>2</sub> foam by use of nanoparticles. *SPE J* 22 (2), 494–504. <https://doi.org/10.2118/174254-PA>.
- Lv, Q., Li, Z., Li, B., Li, S., Sun, Q., 2015. Study of nanoparticle-surfactant-stabilized foam as a fracturing fluid. *Ind. Eng. Chem. Res.* 54 (38), 9456–9477. <https://doi.org/10.1021/acs.iecr.5b02197>.
- G.A. Al-muntasher, E. Advanced, and S. Aramco, "Nanoparticle-enhanced hydraulic-fracturing fluids : a review," no. May 2017.
- Cote, L.J., Kim, J., Tung, V.C., Luo, J., Kim, F., Huang, J., 2011. Graphene oxide as surfactant sheets. *Pure Appl. Chem.* 83 (1), 95–110. <https://doi.org/10.1351/PAC-CON-10-20-25>.
- Kim, J., Cote, L.J., Kim, F., Yuan, W., Shull, K.R., Huang, J., 2010. Graphene oxide sheets at interfaces. *J. Am. Chem. Soc.* 132 (23), 8180–8186. <https://doi.org/10.1021/ja102777p>.
- Barrabino, A., Holt, T., Lindeberg, E., 2018. An evaluation of graphene oxides as possible foam stabilizing agents for CO<sub>2</sub> based enhanced oil recovery. *Nanomaterials* 8 (8). <https://doi.org/10.3390/nano8080603>.
- Szabries, M., Sergelius, S., Kordts, A., Jönsson, M., 2019. Foam stability and foam structure under high pressure for tertiary oil production. *Appl. Rep.* 1–5.
- Maini, B.B., Ma, V., 1986. PRESSURES laboratory evaluation of foaming agents elevated temperatures and pressures. *J. Can. Pet. Technol.* (December).
- Ahmed, S., Elraies, K.A., Hashmet, M.R., Hanamertani, A.S., 2017. Viscosity models for polymer free CO<sub>2</sub> foam fracturing fluid with the effect of surfactant concentration, salinity and shear rate. *Energies* 10 (12), 12–17. <https://doi.org/10.3390/en10121970>.
- Gu, M., Mohanty, K.K., 2015. Rheology of polymer-free foam fracturing fluids. *J. Pet. Sci. Eng.* 134, 87–96. <https://doi.org/10.1016/j.petrol.2015.07.018>.
- Ranjani, G.I.S., Ramamurthy, K., 2010. Analysis of the foam generated using surfactant sodium lauryl sulfate. *Int. J. Concr. Struct. Mater.* 4 (1), 55–62. <https://doi.org/10.4334/ijcsm.2010.4.1.055>.
- Bera, A., Mandal, A., Belhaj, H., Kumar, T., 2017. Enhanced oil recovery by nonionic surfactants considering micellization, surface, and foaming properties. *Pet. Sci.* 14 (2), 362–371. <https://doi.org/10.1007/s12182-017-0156-3>.
- Li, L., Al-Muntasher, G.A., Liang, F., 2016. A review of crosslinked fracturing fluids prepared with produced water. *Petroleum* 2 (4), 313–323. <https://doi.org/10.1016/j.petlm.2016.10.001>.
- Ranka, M., Brown, P., Hatton, T.A., 2015. Responsive stabilization of nanoparticles for extreme salinity and high-temperature reservoir applications. *ACS Appl. Mater. Interfaces* 7 (35), 19651–19658. <https://doi.org/10.1021/acsm.nano804200>.
- Simjoo, M., Rezaei, T., Andrianov, A., Zitha, P.L.J., 2013. Foam stability in the presence of oil: effect of surfactant concentration and oil type. *Colloids Surf. A Physicochem. Eng. Asp.* 438, 148–158. <https://doi.org/10.1016/j.colsurfa.2013.05.062>.
- Azdarpour, A., Rahmani, O., Mohammadian, E., Parak, M., Daud, A.R.M., Junin, R., 2013. The effects of polymer and surfactant on polymer enhanced foam stability. In: BEIAC 2013 - 2013 IEEE Bus. Eng. Ind. Appl. Colloq., pp. 97–102. <https://doi.org/10.1109/BEIAC.2013.6560275>.
- Alooghereh, M.H., Kabipour, A., ghazavi, M., Mohammad Mousavi Sisakht, S., Razavifar, M., 2021. Effects of different gases on the performance of foams stabilized by Cocamidopropyl betaine surfactant and silica nanoparticles: a comparative experimental study. *Petroleum* (xxxx). <https://doi.org/10.1016/j.petlm.2021.09.002>.
- Rio, E., Drenckhan, W., Salonen, A., Langevin, D., 2014. Unusually stable liquid foams. *Adv. Colloid Interface Sci.* 205, 74–86. <https://doi.org/10.1016/j.cis.2013.10.023>.
- C. Park, "A systematic analysis of foam drainage and stability : measurements, mechanisms, and implications for anaerobic digester foaming copyright 2014 by Chanhyuk Park," 2014.
- Abdelgawad, K.Z., 2022. A literature review of strength and stability of foam and their relationship with the absolute permeability of porous media. *J. Pet. Sci. Eng.* 211, 110195.
- Carn, F., Colin, A., Pitois, O., Vignes-Adler, M., Backov, R., 2009. Foam drainage in the presence of nanoparticle-surfactant mixtures. *Langmuir* 25 (14), 7847–7856. <https://doi.org/10.1021/la900414q>.
- Pitois, O., Fritz, C., Vignes-Adler, M., 2005. Liquid drainage through aqueous foam: study of the flow on the bubble scale. *J. Colloid Interface Sci.* 282 (2), 458–465. <https://doi.org/10.1016/j.jcis.2004.08.187>.
- Sharma, M.K., Shah, D.O., Brigham, W.E., 1985. The influence of temperature on surface and microscopic properties of surfactant solutions in relation to fluid displacement efficiency in porous media. *AIChE J* 31 (2), 222–228. <https://doi.org/10.1002/aic.690310208>.
- Minsky, H., Times, N.Y., 2023. The Stability /instability of Bubbles and Foams.

- Messaâdi, A., et al., 2015. A new equation relating the viscosity arrhenius temperature and the activation energy for some newtonian classical solvents. *J. Chem.* 2015, 7–10. <https://doi.org/10.1155/2015/163262>.
- Farajzadeh, R., Krastev, R., Zitha, P.L.J., 2008. Foam films stabilized with alpha olefin sulfonate (AOS). *Colloids Surf. A Physicochem. Eng. Asp.* 324 (1–3), 35–40. <https://doi.org/10.1016/j.colsurfa.2008.03.024>.
- Piskulich, Z.A., Mesele, O.O., Thompson, W.H., 2019. Activation energies and beyond. *J. Phys. Chem. A* 123 (33), 7185–7194. <https://doi.org/10.1021/acs.jpca.9b03967>.
- Bikerman, J.J., 1973. Foam drainage. *Foams* 159–183. [https://doi.org/10.1007/978-3-642-86734-7\\_6](https://doi.org/10.1007/978-3-642-86734-7_6).
- Teixeira, P.I.C., Fortes, M.A., 2007. Energy and tension of films and Plateau borders in a foam. *Colloids Surf. A Physicochem. Eng. Asp.* 309 (1–3), 3–6. <https://doi.org/10.1016/j.colsurfa.2007.02.042>.
- Lin, T.J., Tsuchiya, K., Fan, L.S., 1998. Bubble flow characteristics in bubble columns at elevated pressure and temperature. *AIChE J* 44 (3), 545–560. <https://doi.org/10.1002/aic.690440306>.
- German, S.R., Edwards, M.A., Ren, H., White, H.S., 2018. Critical nuclei size, rate, and activation energy of H<sub>2</sub> gas nucleation. *J. Am. Chem. Soc.* 140 (11), 4047–4053. <https://doi.org/10.1021/jacs.7b13457>.
- Langevin, D., 2019. Coalescence in foams and emulsions: similarities and differences. *Curr. Opin. Colloid Interface Sci.* 44, 23–31. <https://doi.org/10.1016/j.cocis.2019.09.001>.
- Anon, “Activation energy of reactions,” 2016.
- C.M. Duarte, “(p, V<sub>m</sub>, T) measurements on liquid and gaseous mixtures near the critical point,” vol. 32, no. 7, pp. 877–889, 2000.
- Zhou, T., Battino, R., 2001. Partial molar volumes of 13 gases in water at 298.15K and 303.15K. *J. Chem. Eng. Data* 46 (2), 331–332. <https://doi.org/10.1021/je000215o>.
- R. David and L.A. Nauze, “Gas bubble behavior in liquid system,” 1972.